Epithelial Reprogramming by OM-89 Enhances Antibiotic Clearance of Uropathogenic *E. coli* in a Bladder Organoid Model

Kathrin Tomasek[#1], Kristina Skurvydaite[1], Gauri Paduthol[*1], Allison M. Burns[*2], Léa Schlunke[*1], Christian Pasquali[3], Mario Romani[†3] & John D. McKinney[†1]

[#] corresponding author; kathrin.tomasek@epfl.ch

* equal contribution

[†] senior authors

[1] Laboratory of Microbiology and Microtechnology, School of Life Sciences (SV), École Polytechnique Fédérale de Lausanne, 1015 Lausanne, Switzerland

[2] Bioinformatics Competence Centre, École Polytechnique Fédérale de Lausanne, 1015 Lausanne, Switzerland

[3] OM Pharma Ltd., Rue du Bois-du-Lan 22, 1217 Meyrin / Geneva, Switzerland

Abstract

Recurrent urinary tract infections (UTIs) are a major clinical burden, driven by the ability of uropathogenic *Escherichia coli* (UPEC) to persist intracellularly. While vaccine and antibiotic alternatives are being explored, strategies that enhance epithelial cell-intrinsic defenses remain limited. Here, we show that OM-89 (Uro-Vaxom®), an *E. coli* lysate, reprograms epithelial antimicrobial responses to enhance intracellular bacterial clearance. Using murine bladder organoids and epithelial monolayers, we demonstrate that OM-89 increases lysosomal acidification and cathepsin activity, promoting trafficking of UPEC into degradative compartments. Unexpectedly, OM-89 also increases epithelial uptake of antibiotics, boosting their intracellular potency and reducing UPEC regrowth after treatment. This dual effect on epithelial immunity and antibiotic accessibility was conserved across multiple UPEC strains and antibiotic classes. These findings position bladder epithelial cells as active players in the host defense and highlight OM-89 as a tool to amplify their antimicrobial potential, offering a promising adjunctive strategy against intracellular bacterial persistence.

Authors contribution

Conceptualization: KT, GP, CP, MR, JDM; Data curation: KT, KS, GP, LS, AMB; Formal analysis: KT, KS, GP, AMB; Funding acquisition: KT, CP, JDM; Investigation: KT, KS, GP, LS, AMB; Methodology: KT, MR; Project administration: KT, MR; Resources: CP, JDM; Supervision: KT, MR, CP, JDM; Validation: KT; Visualization: KT, AMB, MR; Writing original draft: KT; Writing review & editing: KT, GP, AMB, CP, MR

Keywords

host–pathogen interactions, intracellular bacterial persistence, uropathogenic *Escherichia coli*, bladder organoids, lysosomal activity, vesicle acidification, OM-89 (Uro-Vaxom®)

Introduction

Urinary tract infections (UTIs) are among the most common bacterial infections. Roughly one-third of all UTI patients experience recurrent episodes following antibiotic therapy, necessitating retreatment and therefore promoting the emergence and spread of antibiotic resistances (Medina and Castillo-Pino 2019; Stracy et al. 2022; Foxman et al. 2000). This clinical challenge represents not only a significant burden for affected individuals but also a broader public health risk through the potential propagation of resistant strains (Murray et al. 2022). Additionally, despite standard-of-care antibiotics, treatment failures may occur due to the limited ability of conventional antibiotics to effectively penetrate, accumulate, or remain within host cells, as well as their inability to reach the targeted intracellular compartments (Chifiriuc et al. 2016; Kamaruzzaman et al. 2017). This is especially important for intracellular pathogens such as uropathogenic *Escherichia coli* (UPEC), the leading causative agent of UTIs, which can persist in protected intracellular niches within the bladder mucosa (Lewis et al. 2016; Nisco et al. 2019; Rosen et al. 2007). UPEC's capacity to invade and survive within bladder epithelial cells allows it to evade immune responses and antibiotic-mediated killing (Mysorekar and Hultgren 2006). Within bladder epithelial cells, UPEC can replicate as intracellular bacterial communities (IBCs) (Anderson et al. 2004), or, once sequestered in phagosomes, the pathogen can escape from lysosomal digestion by neutralizing the pH resulting in bacterial expulsion (Miao et al. 2015). Alternatively, UPEC can trigger entry into autophagosomes where bacteria persist in a dormant state as quiescent intracellular reservoirs (QIRs) (Mulvey et al. 2001). These mechanisms contribute to long-term persistence and recurrence (Mysorekar and Hultgren 2006). The molecular mechanism of formation and maintenance of these reservoirs are only partially understood. Important mediators include both bacterial virulence factors, such as type 1 pili (Wright et al. 2007), as well as host cell biology, particularly differentiation status and cytoskeletal architecture (Eto et al. 2006). Rearrangement of the actin cytoskeleton during bladder epithelial differentiation may serve as a cue for bacterial reactivation, linking tissue dynamics to disease recurrence (Blango et al. 2014).

While systemic immunity plays a crucial role in infection control, it is often insufficient to eradicate bacteria hidden within host cells. The bladder epithelium itself functions as an active immunological barrier, capable of sensing infection and mounting antimicrobial responses (Abraham and Miao 2015). Strategies that enhance epithelial cell-intrinsic defenses (Bergman et al. 2020), especially interfering with intracellular UPEC trafficking or enhancing host epithelial antimicrobial responses, represent promising adjunct or alternative strategies to antibiotics to prevent the establishment of persistent intracellular niches. However, host-directed interventions that specifically target epithelial antimicrobial capacity remain scarce.

OM-89, sold under the brand name Uro-Vaxom®, is an orally delivered lysate of 18 *E. coli* strains which is clinically approved for the prevention of recurrent UTIs and as co-medication for the treatment of acute infections (Frey et al. 1986; Bauer et al. 2005). OM-89 modulates immune responses by stimulating the intestinal mucosa, leading to activation of dendritic cells, macrophages, and B and T lymphocytes (Bessler et al. 2009; Huber et al. 2000). However, a recent *in vivo* study combining OM-89 with antibiotic treatment did not find any changes in immune cell responses nor immune cell infiltration in the bladder although recurrence was reduced (Canton et al. 2025). Interestingly, OM-89's respiratory analog OM-85 (Broncho-Vaxom®), a bacterial lysate of 21 bacterial strains frequently responsible for respiratory infections, has been shown to exert direct protective effects on airway epithelial cells, suggesting that mucosal conditioning may extend to distal barrier tissues (Roth et al. 2017). These data, together with pharmacokinetic studies that show the accumulation of OM-89 in the urine (van Dijk 1982), suggests the bladder epithelium as a potential effector site.

Using murine bladder organoids (Sharma et al. 2021) and bladder epithelial cell monolayers derived thereof, we dissected bladder epithelial cell responses to OM-89 under conditions of UPEC infection and antibiotic treatment. These new findings indicate that OM-89 enhances lysosomal activity and antibiotic uptake, leading to accelerated intracellular bacterial clearance and impaired regrowth of the pathogen. Notably, this protective effect was observed across multiple UPEC strains and was independent of the antibiotic's class or mode of action. Our findings reveal a previously unrecognized mechanism by which OM-89 enhances epithelial antimicrobial defenses, positioning the bladder epithelium as an active therapeutic target in recurrent UTI management.

Results

OM-89 reduces regrowth of UPEC strain CFT073 in mouse bladder organoids by enhancing antibiotic-mediated killing

To investigate the effect of OM-89 on bladder epithelial cells and its potential role in reducing UTI regrowth after antibiotic treatment, we used mouse bladder organoids (Sharma et al. 2021) infected with the well-characterized UPEC strain CFT073 (Mobley et al. 1990) – isolated from a pyelonephritis patient. We monitored bacterial growth, antibiotic-mediated killing, and post-treatment regrowth within the organoids. To model clinically relevant treatment scenarios with Uro-Vaxom, we applied OM-89 under three different regimens (Figure 1A): (i) pre-application – OM-89 exposure for 72 hours followed by a 24-hour rest period before microinjection of UPEC; (ii) co-application – OM-89 exposure initiated at the same time as antibiotic treatment; and (iii) continuous application – OM-89 exposure both 72 hours before microinjection and throughout the entire experiment. Notably, OM-89 did not influence bacterial loads during the initial infection phase compared to the PBS control groups (4 h post-infection (pi); SI Figure 1A-C), indicating no antimicrobial effects of OM-89 itself. However, OM-89 significantly reduced bacterial regrowth three hours post-antibiotic treatment (10h pi; 10x MIC of ampicillin) compared to the PBS control in all three treatment regimens (Figure 1B-D), with the effect being most pronounced when OM-89 was present during the antibiotic treatment phase (co-application, Figure 1C; and continuous application, Figure 1D). These positive effects persisted up to eight hours post-antibiotic withdrawal in the continuous application regime (15h pi; Figure 1E).

We next examined the effect of OM-89 during antibiotic treatment (7h pi). While the pre-application regimen showed modest modulation of antibiotic effects (Figure 1F), bacterial loads within organoids were significantly reduced in conditions where OM-89 was present at the time of antibiotic treatment (co-application, Figure 1G; continuous application, Figure 1H). Following bacterial burden in individual organoids in the continuous application regime over time, we observed that OM-89 consistently enhanced bacterial clearance throughout antibiotic treatment and regrowth phases (SI Figure 1D).

To further investigate OM-89's effect, we focused on the continuous application regimen for the rest of the manuscript. First, given the enhanced antibiotic-mediated killing in OM-89-treated cells, we asked if OM-89 could alter antibiotic penetration or accumulation inside bladder epithelial cells, as many conventional antibiotics, including β-lactam antibiotics such as ampicillin, display low intracellular accumulation levels (Carryn et al. 2003). We therefore examined the uptake of fluorescently labeled ampicillin into differentiated monolayers of mouse bladder epithelial cells (SI Figure 2) and observed significantly increased accumulation in bladder epithelial cells treated with OM-89 (Figure 1I). This effect extended to gentamicin, an aminoglycoside antibiotic with usually slow and insufficient intracellular accumulation dynamics commonly used in infection assays to eradicate only extracellular bacteria (Kadurugamuwa and Beveridge 1998; Carryn et al. 2003; Elsinghorst 1994) (SI Figure 1E). It is important to note that the TFP ester of the fluorescent dye used to label ampicillin and gentamicin preferentially reacts with the non-protonated form of free amine groups, which may alter the antibiotics' intracellular behavior and potentially affect their antimicrobial activity. Nonetheless, OM-89 treatment led to increased intracellular accumulation of both antibiotics, as well as Dextran-TMR, a polysaccharide uptake marker (SI Figure 1F), suggesting a generalized enhancement of cellular uptake in bladder epithelial cells compared to PBS-treated controls.

To determine whether the increased uptake of antibiotics contributed to OM-89's protective effect, we reduced the antibiotic concentration from 10-fold to 1-fold the MIC. Even under these conditions, OM-89 maintained its ability to significantly enhance bacterial killing within three

hours (7h pi) and suppress regrowth up to three hours post-treatment (10h pi) (Figure 1J), suggesting that OM-89 improves antibiotic efficacy potentially by increasing intracellular accumulation.

OM-89 modulates immune-related pathways, restores inhibited autophagic flux and upregulates lysosomal pathways in bladder epithelial cells

To further investigate the mode of action of OM-89 at the urothelial cell level, we performed RNA sequencing. Principal component analysis revealed a strong separation between control and infected organoids, and, strikingly, a significant separation was also observed in OM-89-exposed organoids suggesting robust transcriptional changes induced by the treatment (Figure 2A). These differences were reflected in differential gene expression throughout conditions (Figure 2B, SI Figure 3A). Gene set enrichment analysis (GSEA) confirmed that CFT073 infection strongly induced pathways associated with inflammation, bacterial immune signaling, and cell death whereas OM-89 treatment attenuated the activation of this gene signatures (Figure 2C, SI Figure 3B). Importantly, cellular responses to different pathogenic stimuli remained elevated in OM-89 treated organoids compared to uninfected controls (SI Figure 3C), indicating that OM-89 did not abolish epithelial immune responses.

GSEA analysis additionally indicated that the lysosomal pathway was the most significantly induced gene signature following OM-89 treatment during infection (Figure 2D) and further gene set enrichment analysis of lysosomal genes confirmed their involvement in OM-89's response to infection (Figure 2E). Although, lysosomal pathways were also among the top 10 upregulated gene sets in uninfected organoids exposed to OM-89 (SI Figure 3C), the strong upregulation of lysosome-associated terms, together with autophagy-related pathways, was driven by the combination of infection and OM-89 treatment, as infection in the PBS control group did not induce upregulation of these pathways (SI Figure 3B). These data suggest that OM-89 promotes pathways linked to intracellular cargo degradation, particularly under infectious conditions.

We next examined whether OM-89 modulates intracellular trafficking of UPEC in differentiated monolayers of mouse bladder epithelial cells during infection. We first focused on the endosomal pathway by analyzing Rab11A and Rab27B, two small GTPases implicated in UPEC expulsion from bladder epithelial cells (Miao et al. 2017). Rab11A marks recycling endosomes (Cox et al. 2000), while Rab27B is involved in endosomal secretion (Izumi 2007) and late endosome/lysosome trafficking (Underwood et al. 2020). OM-89 treatment significantly increased the number of Rab11A- and Rab27B-positive vesicles, without affecting vesicle size (Figure 3A, 3B).

To assess autophagy responses to OM-89 during UPEC infection, we next quantified canonical autophagy markers (Tanida et al. 2008; Kumar et al. 2022). OM-89 significantly increased both the number and size of ubiquitin-binding protein p62 vesicles (Figure 3C), suggesting enhanced cargo sequestration into autophagosomes. In parallel, OM-89 did not significantly change the number of microtubule-associated protein 1A/1B-light chain 3B (LC3b) vesicles, but it significantly increased LC3b vesicle size (Figure 3D), indicating the formation of larger autophagosomes. To determine whether these morphological changes translated into altered autophagic flux, we performed immunoblotting for membrane-bound LC3b-II in the presence and absence of bafilomycin A1. In PBS-treated bladder epithelial cells, UPEC infection stalled flux, as membrane-bound LC3b-II levels did not increase further upon lysosomal inhibition (Figure 3E), consistent with previously described mechanisms of UPEC-mediated autophagy blockade (Li et al. 2024). In contrast, OM-89 treatment overruled this

pathogen-induced stalling, as LC3b-II accumulated significantly with bafilomycin A1, demonstrating restoration of autophagic flux upon OM-89 treatment during UPEC infection.

Finally, we assessed late endosomal (Vanlandingham and Ceresa 2009) and lysosomal markers (Eskelinen 2006). OM-89 treatment substantially increased both the number and size of Rab7-positive vesicles, consistent with the expansion of the late endosomal compartment (Figure 3F). Lysosomal-associated membrane protein 1 (Lamp1)-positive vesicles were also strongly increased in number; however, their size was reduced (Figure 3G), potentially indicating remodeling of the lysosomal network.

These data suggest that OM-89 promotes autophagosome expansion while overcoming UPEC-mediated stalling of autophagic flux, and enhances lysosomal biogenesis and reorganization during infection.

Lysosomal activation mediates reduction of UPEC regrowth following OM-89 treatment

To understand the potential therapeutic role of OM-89 inducing lysosomal pathways, we first employed Genebridge analysis (Li et al. 2019) to explore correlations between the lysosomal gene expression signature identified in our RNA-seq data. Module-Module association analysis performed on eight human bladder datasets indicated that the lysosome module has strong positive associations with immune response and bacterial defenses modules (Figure 4A), highlighting a functional link between lysosomal activity and immune defense pathways in the bladder epithelium.

To further investigate the role of lysosomal modulation in OM-89 mediated effects against UPEC infection, we examined the involvement of lysosomal activity and intracellular pH. In line with remodeling of the late endosomal and lysosomal network (Figure 3F, 3G), OM-89 treatment led to a significant increase in the number of enlarged acidic vesicles (Figure 4B), accompanied by a significant reduction in overall intracellular pH (Figure 4C). Notably, while CFT073 infection elevated intraorganellar pH in PBS-treated controls (pH of 7.5 ± 0.38) compared to uninfected controls (pH of 7.0 ± 0.24), consistently with pathogen-mediated disruption of vesicle acidification (Naskar et al. 2023; Miao et al. 2015), OM-89 treatment maintained a more acidic environment in both conditions (pH of 6.58 ± 0.35 during infection and 6.45 ± 0.28 without infection; Figure 4C, SI Figure 4A). When focusing on intracellular UPEC, OM-89-treated cells showed a significant increase in signal intensity of acidic compartments (Figure 4D), Lamp1-positive vesicles (Figure 4E) and enzymatically active lysosomes (cathepsin L-positive vesicles; Figure 4F) in close proximity to internalized bacteria compared to PBS controls. While OM-89 expanded Lamp1- and LysoTracker-positive compartments (Figure 3G, 4B), colocalization of intracellular UPEC with these markers was largely proportional to vesicle abundance and consistent with stochastic overlap (enrichment scores ≈1 or <1) (Figure 4D, 4E and SI Figure 4B, 4C). However, OM-89 significantly increased the enrichment of UPEC in proximity to cathepsin L-positive vesicles (enrichment score 1.25 in OM-89 vs 0.91 in PBS) (Figure 4F, SI Figure 4D), indicating enhanced routing of UPEC into proteolytically competent autolysosomes. Overall, OM-89-treated bladder epithelial cells exhibited significantly elevated cathepsin L levels in the presence of infection (SI Figure 4E), indicating that the highly abundant acidic and lysosomal compartments were functionally active. Since lysosomal proteases such as cathepsins require an acidic environment for activation of their antimicrobial effects against intracellular bacteria (Szulc-Dąbrowska et al. 2020), we next aimed to abolish acidification with pharmacological inhibition. Bafilomycin A1 (Mauvezin and Neufeld 2015) collapsed the OM-98-driven enrichment of intracellular UPEC in proximity to cathepsin L-positive vesicles to PBS-control levels, demonstrating a clear

acidification dependence (Figure 4G, SI Figure 4F). Overall, bafilomycin A1 or chloroquine (Mauthe et al. 2018) treatment reduced cathepsin activity to comparable levels in OM-89- and PBS-treated cells (SI Figure 4E). Interestingly, chloroquine treatment led to a partial increase in cathepsin activity, particularly in infected PBS-treated cells.

Finally, given the enhanced lysosomal function and increased localization of intracellular UPEC to protease active compartments during OM-89 treatment, we next asked whether this effect was essential for OM-89-mediated protection. Importantly, inhibition of acidification using either bafilomycin A1 or chloroquine did not affect initial bacterial load during infection in OM-89-treated versus PBS-treated organoids (SI Figure 4G, 4H). However, blocking acidification using either of the two inhibitors fully abolished OM-89's protective effect, restoring bacterial regrowth to levels observed in PBS-treated controls (Figure 4H, 4I; 10h pi – regrowth). Interestingly, while OM-89 still promoted antibiotic-mediated killing in bafilomycin A1-treated organoids (Figure 4H, killing), this effect was completely lost with chloroquine treatment (Figure 4I, 7h pi – killing).

These findings indicate that OM-89's antimicrobial effects on bacterial clearance strongly relies on lysosomal acidification and therefore full protease activity.

OM-89 reduces regrowth following treatment with different antibiotics and across multiple UPEC strains

To validate OM-89's ability to reduce regrowth of CFT073 after clinically relevant antibiotic exposure, we investigated its effect following treatment with antibiotics that have different mechanisms of action than ampicillin and different intracellular accumulation levels (Carryn et al. 2003; Bongers et al. 2019). We selected two commonly prescribed antibiotics for uncomplicated UTIs: Fosfomycin (FOS), a bacterial cell wall-targeting antibiotic displaying weak host cell accumulation (Höger et al. 1985) and trimethoprim/sulfamethoxazole (TMP-SMX), a folate synthesis inhibitor showing more effective intracellular accumulation (Bongers et al. 2019). OM-89 effectively reduced regrowth of CFT073 in bladder organoids (10h pi) after both FOS (Figure 5A) and TMP-SMX (Figure 5B) treatment and enhanced the killing (7h pi), indicating that its effect on bladder epithelial cells is independent of the antibiotic's mode of action and accumulation levels.

Finally, we assessed the regrowth of two additional well-characterized UPEC strains, UTI89 (a cystitis isolate) (Chen et al. 2006) and J96 (a pyelonephritis isolate) (Klein and Gitai 2013), following ampicillin treatment. As observed with CFT073, OM-89 significantly enhanced killing (7h pi) of both UTI89 (Figure 5C) and J96 (Figure 5D) leading to reduced regrowth (10h pi), without affecting their initial growth within the organoids (SI Figure 5A, 5B).

OM-89 therefore affects regrowth across multiple UPEC strains and following treatment with different antibiotics.

Discussion

Intracellular reservoirs of UPEC within bladder epithelial cells are a key driver of recurrent UTIs due to their evasion of both antibiotics and immune responses (Mysorekar and Hultgren 2006). Using OM-89 as a tool to probe epithelial plasticity, we show that urothelial cells can be reprogrammed to enhance intracellular clearance of UPEC by upregulation of lysosomal pathways and by improving antibiotic uptake, without compromising immune responses. These new findings highlight host-directed modulation of epithelial responses at the site of infection – the urothelium – as a promising strategy to reduce relapse of infection.

Here, we demonstrate that OM-89 treatment mediated coordinated remodeling of endosomal and lysosomal compartments in bladder epithelial cells during UPEC infection. The number of recycling and secretion-associated vesicles (Rab11A, Rab27B) were increased, consistent with enhanced endosomal turnover and pathways implicated in bacterial expulsion (Miao et al., 2017). Although p62 vesicles accumulated, a potential sign of intracellular stress (Kumar et al. 2022), the observed enlarged autophagosomes together with increased autophagic flux indicate enhanced sequestration of the ubiquitinated cargo and processing towards active autolysosomes. With this, OM-89 enables bladder epithelial cells to overcome UPEC-mediated stalling of autophagic flux (Li et al. 2024). This is also reflected in enlargement of Rab7-positive late endosomes and increased Lamp1-positive vesicle numbers, both indicative of increased lysosomal biogenesis and remodeling.

Importantly, although the smaller size of Lamp1-positive vesicles could be due to induced lysosomal fragmentation by UPEC via secretion of α-hemolysin (HlyA) (Naskar et al. 2023), OM-89 shifted the balance toward increased routing to functionally degradative compartments, to enhance intracellular clearance: OM-89 both expanded the lysosomal network and functionally mobilized lysosomal proteases to pathogen-containing compartments. While Lamp1 and LysoTracker signals increased globally inside bladder epithelial cells raising stochastic overlap, functional cathepsin activity was specifically concentrated in the proximity of intracellular UPEC. This indicates enhanced routing of intracellular pathogens into proteolytically competent autolysosomes and provides a mechanistic basis for improved bacterial clearance in the presence of additional antibiotic stress. Chemical inhibition of lysosomal acidification using bafilomycin A1 and chloroquine abrogated OM-89's protective effect, establishing a causal link between lysosomal function and reduced bacterial regrowth. Together, these findings indicate that OM-89 enhances lysosomal acidification and degradative capacity, thereby trafficking UPEC into more numerous, functionally degrative compartments. This remodeling of epithelial vesicular trafficking likely counteracts bacterial strategies to evade degradation (Naskar et al. 2023; Miao et al. 2015) and highlights a yet underappreciated mechanism of OM-89 in fine-tuning epithelial immunity to strike a balance between pathogen clearance and tissue integrity.

Notably, this enhancement of host antimicrobial activity was not sufficient to limit UPEC replication during the initial infection phase, suggesting that OM-89's protective mechanism requires additional context, specifically, antibiotic treatment. We found that OM-89 enhanced intracellular accumulation of antibiotics. While chemical labeling of ampicillin and gentamicin via their free amine groups may alter their biophysical properties, the consistent increase in intracellular signal across two structurally distinct, poorly permeant antibiotics strongly suggests that OM-89 broadly improves epithelial uptake or their retention. Furthermore, ampicillin and gentamicin differ significantly in their intracellular pharmacokinetics: Ampicillin can pass across membranes but displays limited accumulation levels, most likely because of the free proton-donor group inherent by β-lactams which favor the more neutral extracellular space compared to the slightly more acidic cytosol (Carryn et al. 2003), whereas gentamicin

diffuses very slowly and poorly through cell membranes due to its high hydrophilicity (Tulkens and Trouet 1978). The observation that OM-89 enhances accumulation of both, as well as the polysaccharide Dextran, supports a generalized increase in intracellular delivery mechanisms, which may reflect altered endocytic or transporter activity. These are important findings, as antibiotics used to treat UTIs span a wide range of classes, like β-lactam antibiotics, fluoroquinolones, Fosfomycin, trimethoprim-sulfamethoxazole and aminoglycosides (Bader et al. 2020) with variable intracellular activity profiles (Carryn et al. 2003; Höger et al. 1985; Bongers et al. 2019). Enhancing intracellular access could substantially improve antibiotics' efficacy against intracellular UPEC. Supporting this, we found that OM-89 reduced bacterial regrowth even at a 10-fold lower ampicillin concentration than otherwise used in this study (1x MIC vs. 10x MIC), highlighting its potential to expand the pharmacodynamic properties of prescribed antibiotics.

Importantly, OM-89's protective effects not only extended across different antibiotic classes, including ampicillin, Fosfomycin and trimethoprim/sulfamethoxazole but also across well-characterized laboratory UPEC strains (CFT073, UTI89, J96). OM-89 consistently affected regrowth after antibiotic withdrawal suggesting that OM-89 can overcome strain-specific differences in intracellular persistence, further supporting its clinical relevance. If OM-89 also exhibits its protective effects against primary clinical isolates of UPEC or other pathogens causing UTIs needs further investigation.

While our study characterized epithelial mechanisms in a well-established mouse bladder model, the next logical step would be to identify whether similar epithelial reprogramming can be achieved in human-derived systems, for example by using 2D organoid-like systems (Zulk et al. 2025). Such systems would assess how OM-89-driven lysosomal activation and enhanced intracellular antibiotic accumulation translate to the human urothelium.

Taken together, our findings demonstrate that uroepithelial cells can be employed as active defenders against intracellular bacterial persistence. OM-89 serves as a proof-of-concept that reprogramming epithelial responses – through enhanced lysosomal activity, intracellular acidification, targeted trafficking of UPEC into degradative compartments, and improved antibiotic accumulation – can significantly limit pathogenic regrowth. By boosting the efficacy of existing antibiotics at the cellular level, such approaches may enable shorter and lower-dose regimens, reducing overall antibiotic exposure. This is particularly critical in the era of antimicrobial resistance, which is projected to surpass cancer and cardiovascular disease as a leading cause of mortality (Global burden of bacterial antimicrobial resistance 1990-2021: a systematic analysis with forecasts to 2050 2024). Epithelial-targeted immunomodulation could therefore represent a powerful adjunct strategy by transforming the bladder epithelium from a reservoir for recurrent infection into an active site of accelerated pathogen clearance, while contributing to global efforts to restrain the rise of resistant bacterial pathogens.

STAR Methods

Bacteria

The well-characterized UPEC strains CFT073 (Mobley et al. 1990), UTI89 (Chen et al. 2006) and J96 (Klein and Gitai 2013) were used. Strains were grown in DMEM/F-12 (Thermo Fisher) supplemented with 20 mM HEPES (Thermo Fisher) without (for organoid injections) or with (for monolayer infections) 10% heat-inactivated Fetal Bovine Serum (FBS, Thermo Fisher) at 37°C statically.

Chromosomal sfGFP integration

To enable real-time monitoring of the infection dynamics, CFT073 and other UPEC strains were genetically engineered to stably express *sfGFP* under control of a strong $P_{\sigma 70}$ promoter at the chromosomal att_{HK022} site using scare-less cloning (Eshaghi et al. 2016; Simonet et al. 2022). Briefly, the kan^R-P_{RhaB}-*relE* toxin cassette was amplified from plasmid pSLC217 using primers P4 and P5 and integrated into the genome of the strains using λ Red recombineering (Datsenko and Wanner 2000). Primers P6 and P7 were then used to amplify the sfGFP-containing fragment from plasmid pSLC293, and these PCR amplicons were used to replace the kan^R-P_{RhaB}-*relE* toxin cassette by λ Red recombineering with negative selection on M9 agar (Sigma) supplemented with 2% L-rhamnose (Sigma). Successful recombination at each step was confirmed by PCR using primers attHK_F and attHK_R.

Used bacterial strains are listed in Table 1. Primers are listed in Table 2.

Strain name	Genotype	Source
TS4	CFT073 *ΔfliC::FRT*	Simonet et al. 2022
TS85	CFT073 att_{HK022}:: σ_{70}-*sfGFP*	Simonet et al. 2022
TS66	TS4 att_{HK022}:: σ_{70}-*sfGFP*	Simonet et al. 2022
FN27	J96 att_{HK022}:: σ_{70}-*sfGFP*	Valentin Borgeat
FN28	UTI89 att_{HK022}::σ_{70}-*sfGFP*	Valentin Borgeat

Table 1. Used strains.

Primer name	Nucleotide sequence (5' to 3')	Source
attHK_F	GCTGATAAAGCGCAGGTTG	this study
attHK_R	GCGCAACAGGTTATCAGC	this study
fliC_KO_F	TAATCAACGACTTGCAATATAGGATAACGAATCATGGCACAATGTG TAGGCTGGAGCTGCTTCG	Thomas Simonet
fliC_KO_R	TGCCGTCAGTCTCAGTTAATCAGGTTACGGCGATTAACCCTGCATA TGAATATCCTCCTTAG	Thomas Simonet
fliC_F	CAGACGATAACAGGGTTGACGGC	Thomas Simonet
fliC_R	TTGCAATTCCCCTTGTAGGCCTG	Thomas Simonet
P4	GCGCCATCAGGGCAAAGCCCATCCAGAGTCTTCGGGTCAGGGTTA AATTCACGGTCGGTGCGTGTAGGCTGGAGCTGCTTC	Eshaghi et al. 2016
P5	ATAATAAGGCTTTATGCTAGATGCATTCTGCTTTGCGACTCAACCTT TTTCACCTAAAGTCATATGAATATCCTCCTTAG	Eshaghi et al. 2016
P6	GCGCCATCAGGGCAAAGCCCATCCAGAGTCTTCGGGTCAGGGTTA AATTCACGGTCGGTGCTTGACGGCTAGCTCAGTCCTA	Eshaghi et al. 2016
P7	ATAATAAGGCTTTATGCTAGATGCATTCTGCTTTGCGACTCAACCTT TTTCACCTAAAGTTTAATGATGATGATGATGATG	Eshaghi et al. 2016

Table 2. Used primers.

Cell culture

Mouse primary bladder epithelial cells were obtained from C57BL/6 mice (Charles River Laboratories) aged 3-4 months or female ROSA$^{MT/MG}$ mice (Jackson Laboratories) at age 4 months. Mice were housed in a specific pathogen-free facility. All animal protocols were reviewed and approved by EPFL's Chief Veterinarian, by the Service de la Consommation et des Affaires Vétérinaires of the Canton of Vaud, and by the Swiss Office Vétérinaire Fédéral. Mouse bladder epithelial cells were routinely grown in mouse bladder organoid (MBO) media as described previously (Sharma et al. 2021).

Routinely, cells were grown at 37°C and 5% CO_2 without antimicrobial or antimycotic agents. Organoids were cultured in either MBO media or DMEM/F-12 media, whereas for monolayers a total of 10% FBS was added to DMEM/F-12 media and plastics were coated with gelatin-based coating solution (ABC Biopply). The day prior to infection, 20 mM of HEPES was added and kept throughout the experiments.

Mouse bladder organoids

Mouse organoids were grown as described (Sharma et al. 2021) with minor modifications. Briefly, the extracted mouse bladders were minced with scissors. The minced tissue was submerged in 1-1.5 mL of pre-warmed TryPLE (Thermo Fisher) and incubated at 37°C at 170 rpm for 30 minutes. After vortexing for 30 seconds, TryPLE was deactivated with DMEM/F-12 supplemented with 10% FBS. Organoids were grown from single cells in reduced growth factor basement membrane extract (BME, BioTech AG) domes in MBO media. Organoids were passaged as single cells extracting organoids from BME domes with cell recovery solution (Corning) and subsequent TryPLE digestion every 5-7 days. MBO media was renewed every 2-3 days and exchanged to DMEM/F-12 media once organoids reached the desired size for microinjections (usually 1-2 days prior to the experiment). For microinjection experiments, tdTomato organoids from ROSA$^{MT/MG}$ mice were used, whereas WT organoids were mainly used for monolayer experiments.

Mouse bladder epithelial cell monolayers

Mouse bladder epithelial cells from WT organoids were broken into single cells by TryPLE treatment. Single cells of mouse bladder epithelial cells were seeded into µ-plate 96-well dishes (ibidi) in MBO media. Upon reaching roughly 40 to 50% confluency, MBO media was replaced with DMEM/F-12 supplemented with 10% FBS for 2-3 days to drive differentiation of cells by depriving them from growth factors. Umbrella-like cells expressed cytokeratin (CK) 20 and uroplakin (UP) 3a, intermediate cells expressed, basal cells expressed CK5 (Jafari and Rohn 2022; Sharma et al. 2021). Umbrella-like cells were frequently binucleated. Differentiated monolayers were used for experiments upon reaching 100% confluency.

OM-89 treatment

Organoids and monolayers were treated with OM-89 at 500 µg/ml of protein in either MBO or DMEM/F-12 media. For control groups, equal volumes of phosphate buffered saline (PBS, Thermo Fisher) was used instead of OM-89. OM-89 and PBS were added to the media according to the different treatment regimes: continuous application – 72 hour treatment pre-infection and treatment throughout the experiment, pre-application – 72 hour treatment pre-infection only with a 24 hour resting period where treatment was omitted, co-application – treatment only during antibiotic treatment. For the continuous application, bacteria were microinjected after adjusting their optical density at 600 nm (OD_{600}) in media with either PBS or OM-89. If not stated other, bladder epithelial cells were subjected to the continuous application and 10x the strain MIC of the indicated antibiotic was used.

Minimal inhibitory concentration (MIC) measurements

Bacteria were grown in DMEM/F-12 with 20 mM HEPES. Overnight cultures were diluted to an OD_{600} of 0.002 and grown till OD_{600} of 0.01. Bacterial cultures were adjusted to an OD_{600} of 0.0005 for serial dilutions of tested antibiotics. MIC was estimated based on growth after 24 hours in a plate reader (Tecan Infinite M Nano) and using the Goempertz equation for MIC determination (Lambert and Pearson 2000) (Table 3).

Strain	Antibiotic	MIC [µg/ml]
CFT073	Ampicillin	6.43
CFT073	Fosfomycin	6.97
CFT073	Trimethoprim/Sulfamethoxazole	1.76
UTI89	Ampicillin	5.35
J96	Ampicillin	9.98

Table 3. MICs.

Injection experiments

tdTomato organoid injections were performed as described (Sharma et al. 2021) with minor modifications. Briefly, on the day prior to the experiments organoids were passaged into µ-slide 2 well ibidi dishes (ibidi) and MBO media was replaced with DMEM/F-12 with 20 mM HEPES. UPEC strains with stable chromosomal integration of *sfGFP* were grown statically in DMEM/F-12 with 20 mM HEPES. On the day of the experiments, the media of the organoids was replaced with fresh media. The OD_{600} of bacterial cultures was adjusted to 2.25 in a 1:1 dilution of media and Phenol Red solution (Sigma-Aldrich) to facilitate the visualization of injected organoids. Microinjections were performed using a Pneumatic PicoPump (WPI) using micropipettes prepared from thin wall glass capillary (TW100F-4 with length 100 mm and diameter 1 mm) using a Flaming/Brown Micropipette Puller (Sutter Instruments model P-87) set at pressure 360, heat 866, Vel 200. The micropipettes were then cut with tweezers under a stereomicroscope (Olympus SZX-16) to generate a tip size ejecting roughly 1 nl volume of the adjusted bacterial culture in mineral oil on a Zeiss coverslide (corresponding to 100 mm), corresponding to 1926 ± 150 colony forming units (CFU) per injection (quantified from two needles, plating three replicates on LB agar plates). Injected organoids were allowed to rest for 1 hour prior to time-lapse microscopy imaging onset.

Time-lapse microscopy

Imaging of infected organoids was conducted using a Leica Thunder DMi8 microscope (Leica) with a temperature-controlled microscope environmental chamber maintained at 37°C and 5% CO_2 in a stage-top chamber (OKOlabs) using a Leica HC FLUOTAR VISIR 25x (NA 0.95) water-immersion objective. To maintain the water immersion for the objective, water was pumped to the ring around the water objective. Microinjected tdTomato-expressing organoids were identified and imaged at ex476/em519 nm (UPEC) and ex554/em594 nm (tdTomato) at 85 ms exposure time, acquiring the multiple channels during the same imaging sequence to improve the temporal resolution. Z stacks were acquired with 1 µm step sizes. Selected organoids were images 4 hours into the infection phase (corresponding to G3 of acquired images), throughout the antibiotic phase where indicated (corresponding to Amp0-3 of acquired images) and 3 hours after antibiotic withdrawal (corresponding to RG3 of acquired images). For experiments indicated, regrowth was observed for longer. UPEC fluorescence area overlapping with organoid area (meaning bacterial signal only from inside the infected organoid by masking the tdTomato signal on the GFP signal; the intra-organoid bacterial signal) was extracted at the indicated time-points using fiji scripts *Volumetric calc_growth* and *Volumetric calc_regrowth*. For analysis, the obtained fluorescence area at any time-point

(growth, antibiotic-mediated killing or regrowth) of the intra-organoid bacterial signal was normalized to the same time-point of the PBS control group within one experiment.

Blocking of acidification

Where indicated, 10 µM chloroquine (CQ, InvivoGen) or 0.1 µM bafilomycin A1 (bafA1, InvivoGen) was added. Usual pre-treatment with either CQ or bafA1 was 3 hours for organoid and monolayer experiments. Afterwards, blocking was washed off with excessive amounts of prewarmed DMEM/F-12 before adding fresh media before UPEC infections. When enhancing for intracellular bacteria, such as co-localization experiments with Cathepsin L, blocking was added 1 hour before infection, and left throughout the infection and Cathepsin L staining (additional 4 hours).

Immunofluorescence staining

Differentiated monolayer staining

Confluent monolayers were fixed with 4% paraformaldehyde (PFA, Thermo Fisher) for 1 hour at 4°C and then washed with PBS. For umbrella-like cells, cells were blocked for 1 hour at room temperature in 1% bovine serum albumin (BSA, Thermo Fisher) before staining with UP3a (mouse anti-UP3a; sc-166808) in 1% BSA in PBS. After washing, cells were permeabilized with 0.1% Triton-X in PBS for 10 minutes. Cells were washed and blocked again before staining with primary antibodies for the main three bladder epithelial cell types: cytokeratin (CK) 5 (rabbit anti-CK5; ab52635) for basal cells, CK13 (rabbit anti-CK13 Alexa Fluor-488; ab198584) for intermediate cells and CK20 (rabbit anti-CK20; orb256650) for umbrella-like cells. Primary antibodies were diluted 1:100 in 1% BSA in PBS. After washing, cells were incubated with 1:1000 dilution of secondary antibody (donkey anti-rabbit Alexa Fluor 647; A-31573) and phalloidin-555 (Thermo Fisher) and DAPI in 1% BSA in PBS. Each staining was carried out for 1 hour at room temperature. Images were taken on a Confocal Stellaris 5 (Leica) using a HC PL APO 63x (NA 1.40) oil-immersion objective.

Vesicle staining

Differentiated monolayers were infected with TS4 at roughly $1*10^6$ CFU/ml for 4 hours. Thereafter, extracellular bacteria were washed with excessive amounts of PBS before fixing. Fixing, permeabilization and staining were carried out as mentioned above. Primary antibodies were LC3b (rabbit anti-LC3b; ab192890), Rab11A (mouse anti-Rab11A; sc-166912), Rab27B (rabbit anti-Rab27B; orb637040), Rab7 (mouse anti-Rab7; sc-376362), Lamp1 (rat anti-Lamp1; sc-19992) and p62 (rabbit anti-SQSTM1; ab109012). Images were taken on a Confocal Stellaris 5 and foci were counted in 3D using fiji script *3D_foci_counting*.

Western blot

Proteins from differentiated monolayers were isolated by resuspending cells after TryPLE digestion in 300 µL Radioimmunoprecipitation assay (RIPA) buffer. The protein mixture was then either used immediately or aliquoted and stored at -80°C. Protein concentrations were measured with the Pierce BCA protein assay kit (Thermo Fisher) and approximately 3 µg of proteins were boiled for 10 min at 70°C with NuPAGE LDS sample buffer (Invitrogen) and Dithiothreitol (DTT, Thermo Fisher) before running them on a 4-12% Bis-Tris gel (Invitrogen). Proteins were transferred onto a membrane using the iBlot Gel Transfer Device (Invotrgen). The membrane was cut to sperate GAPDH and LC3b bands and the membrane part containing LC3b (15-17 kDA) was pretreated with SuperSignal West Atto substrate solution (ThermFisher). After blocking both membrane parts for 1 hour at room temperature with 1% BSA in Tris-buffered saline (TBS), they were incubating with primary antibodies overnight at 4°C – GAPDH (ab181602) 1:2000 in 2% BSA in TRIS-NaCl-Tween 20 (TNT) buffer; LC3b

(ab192890) 1:1000 in SuperSignal western blot enhancer (Thermo Fisher). After washing with TBS, blots were incubated with secondary antibody (polyclonal goat anti-rabbit Immunoglobular HRP; Dako 41653919) 1:2000 in 2% BSA in TNT for 1 hour at room temperature prior to visualizing signals with SuperSignal West Pico PLUS chemiluminescent substrate (Thermo Fisher).

Uptake assays

Dextran-TMR uptake

Differentiated monolayers were incubated with fixable Dextran Tetramethylrhodamine (Dextran-TMR; Thermo Fisher) at a final concentration of 1 mg/ml for 4 hours before repeated washes with PBS and fixation with 4% PFA for 1 hour at 4°C. Images were taken on a Confocal Stellaris 5 and intracellular fluorescence was extracted after background subtraction of PBS or OM-89-treated cells using fiji.

Labelled antibiotic uptake

Ampicillin and gentamycin were labelled using Pierce™ FITC Antibody Labeling Kit (Thermo Fisher) according to the manufacturer's recommendations. Labelled stocks at 2 mg/ml of each antibiotic were aliquoted and stored at -20°C. Differentiated monolayers were incubated with FITC-labelled ampicillin and gentamycin for 3 hours a final concentration of 64.5 µg/ml (10x MIC of CFT073 for ampicillin) and 100 µg/ml (usual concentration used for gentamicin protection assays (Mulvey et al. 2001)) respectively. Excess FITC-labelled antibiotic was washed off with repeated PBS washes before taking images on a Confocal Stellaris 5. Intracellular fluorescence was extracted after background subtraction of PBS or OM-89-treated cells using fiji.

Colocalization of intracellular UPEC with acidic compartments, Lamp1 and Cathepsin L

Differentiated monolayers were infected with TS66 at roughly $1*10^6$ CFU/ml for 4 hours on a rocking platform to facilitate bacterial uptake for intracellular bacteria imaging. Thereafter, extracellular bacteria were washed with excessive amounts of PBS. For staining of acidic compartments, cells were incubated with LysoTracker DND-99 Red (Thermo Fisher) at 50 nM for 30 min following manufacturer's recommendations. Thereafter, monolayers were fixed with 4% PFA for 1 hour at 4°C and stained phalloidin and DAPI as mentioned above. For staining of Lamp1-positive vesicles, cells were fixed and stained with Lamp1 antibody, phalloidin and DAPI as mentioned above. For staining of enzymatically active compartments, Cathepsin L activity stained using Magic Red™ Cathepsin L kit (bio-rad) following manufacturer's recommendations. After 3 hours of infection, the Magic Red™ substrate and NucBlue™ Live ReadyProbes™ Reagent (Hoechst 33342, Thermo Fisher) was added on top for 60 min. After washing 3 times, cells were stained with CellMask™ Plasma Membrane Stain in Deep Red (Thermo Fisher) for 10 minutes. After washing again, cells were briefly fixed with 4% PFA for 15 min at RT. Cells were imaged on a Confocal Stellaris 5. Intracellular bacteria were cropped by segmenting on bacterial signal inside the phalloidin signal of the bladder epithelial cells in fiji using the orthogonal view. Colocalization of intracellular bacteria with either LysoTracker, Lamp1 or Cathepsin L signal was then analyzed using the fiji script *fluorescent_overlap_intracellular_bacteria* by drawing a freehand region of interest (ROI) around bacteria and extracting the mean fluorescence intensity normalization over the area of the ROI. For random control ROIs, images were processed the same way except for moving the ROI from the bacterial cluster to an area without bacterial signal.

Intraorganell pH

The intraorganell pH of differentiated monolayers was estimated using LysoSensor™ Yellow/Blue DND-160 (Thermo Fisher) following manufacturer's recommendations with minor modifications. Briefly, LysoSensor was diluted to a final concentration of 5 µM in live cell imaging solution (140 mM NaCl, 2.5 mM KCl, 1.8 mM $CaCl_2$, 1.0 mM $MgCl_2$, 20 mM HEPES, pH 7.4). Mouse bladder epithelial cells were incubated for 10 min with the sensor before measuring fluorescent intensity on a plate reader (Tecan Infinite M Nano) taking four measurements per well.

Cathepsin assay

Cathepsin L activity in differentiated monolayers was measured using Magic Red™ Cathepsin L kit (bio-rad) following manufacturer's recommendations. Cells were incubated with Magic Red™ substrate for 60 min and fluorescent intensity was measured on a plate reader (Tecan Infinite M Nano) taking four measurements per well.

RNA extraction and sequencing

Organoids were either left uninfected or were infected as described above. Four hours after microinjection the organoids were extracted from the BME using cell recovery solution. For RNA extraction, organoids were incubated with the appropriate volume of RNA lysis buffer (RNAeasy Plus Mini Kit, QIAGEN) and RNA was isolated following the manufacturer's instructions. RNA quantification and quality control was performed on a TapeStation 4200 (Agilent). Libraries were prepared using the "Illumina stranded mRNA ligation" (ISML) prep, according to Illumina protocol 1000000124518 v01. To account for bacterial mRNA contaminations during the mRNA polyA capture step, 200 ng of RNA for the PBSinf samples was used due to the presence of a double set of rRNA peaks whereas for all other samples 125 ng of RNA was taken. Libraries were then sequenced on the NovaSeq 6000 (Illumina) yielding approximately 25-35 million, 60-bp, paired end reads for all samples.

RNA sequencing analysis

STAR (v.2.7.10b) (Dobin et al. 2013) was used to align FASTQ reads to the mouse mm10 reference genome and count reads in genes from the annotations in Ensembl release 102. Genes were considered expressed and maintained for downstream analysis if they had more than 10 counts in at least 4 of the samples (14,114 genes remaining). Differential expression analysis was performed using DESeq2 (version 1.36.0) and genes were considered differentially expressed if they were changed by more than 2-fold (log2FC ≥ 1) and had a corrected p-value ≤ 0.05. Two methods were used for exploring affected pathways: first, an over-representation analysis, using the g:Profiler (Kolberg et al. 2023) R client, was used to determine which pathways were enriched for up and down-regulated genes separately. For the gene set enrichment analysis, all expressed genes were ranked by their wald statistic and analyzed using the fgsea toolset in R (Korotkevich et al. 2016) for both GO and KEGG databases.

Genebridge MMAS analysis

Genebridge MMAS (Module-Module Association Score) within the GeneBridge platform was used to identify and quantify connections between different biological modules (Li et al. 2019). Briefly, GeneBridge uses cross-species transcriptome compendia and statistical analysis to determine the significance of relationships between modules. We analyzed the KEGG lysosomal category to identify models positively correlating with it in eight human bladder datasets.

Statistical analysis

Statistics were performed with GraphPad Prism 10.3.1. Data and corresponding test results (e.g., normality results, T-values, degrees of freedoms, p-values) can be found in Supplementary Information.

Data availability

Raw RNA-sequencing data have been deposited in the Gene Expression Omnibus (GEO) under accession number GSE306613. All other data supporting the findings of this study, including processed datasets, Fiji scripts, and linked statistical analyses, will be made available on Zenodo (DOI: 10.5281/zenodo.17413104).

Competing interests

M.R. was and C.P. is an employee of OM Pharma SA, Meyrin, Switzerland. All other authors declare that they have no conflict of interest.

Acknowledgements

We thank Valentin Borgeat, Dr. Ophélie Rutschmann and Mathilde Morelli for experimental and technical support; Dr. Naomi Wieser and Dr. Edouard Baulier from OM Pharma, as well as all of the McKinney laboratory for helpful discussions; the Gene Expression Core Facility at EPFL for RNAseq data generation; and the BioInformatics Competence Center, University of Lausanne and EPFL for analysis of the RNAseq data. K.T. acknowledges support from a Swiss Government Excellence Scholarship (2022.0289), a Swiss National Science Foundation (SNSF) Postdoctoral Fellowship (TMPFP3_217144) and support from the IBSA Foundation. This research was supported by a grant to J.D.M. from the National Centre of Competence in Research (NCCR) AntiResist funded by the SNSF (grant number 51NF40_180541). OM Pharma supported this study by providing funding to K.S. and by providing OM-89.

Declaration of generative AI and AI-assisted technologies in the manuscript preparation process

During the preparation of this work the author(s) used ChatGPT (OpenAI) in order to assist with language refinement and clarity in sections of the manuscript, including improving phrasing, grammar, and flow. After using this tool/service, the author(s) reviewed and edited the content as needed and take(s) full responsibility for the content of the published article.

References

Abraham, Soman N.; Miao, Yuxuan (2015): The nature of immune responses to urinary tract infections. In Nature reviews. Immunology 15 (10), pp. 655–663. DOI: 10.1038/nri3887.

Anderson, Gregory G.; Dodson, Karen W.; Hooton, Thomas M.; Hultgren, Scott J. (2004): Intracellular bacterial communities of uropathogenic Escherichia coli in urinary tract pathogenesis. In Trends in microbiology 12 (9), pp. 424–430. DOI: 10.1016/j.tim.2004.07.005.

Bader, Mazen S.; Loeb, Mark; Leto, Daniela; Brooks, Annie A. (2020): Treatment of urinary tract infections in the era of antimicrobial resistance and new antimicrobial agents. In Postgraduate medicine 132 (3), pp. 234–250. DOI: 10.1080/00325481.2019.1680052.

Bauer, Hartwig W.; Alloussi, Schanaz; Egger, Günther; Blümlein, Hans-Martin; Cozma, Gabriel; Schulman, Claude C. (2005): A long-term, multicenter, double-blind study of an Escherichia coli extract (OM-89) in female patients with recurrent urinary tract infections. In European urology 47 (4), 542-8; discussion 548. DOI: 10.1016/j.eururo.2004.12.009.

Bergman, Peter; Raqib, Rubhana; Rekha, Rokeya Sultana; Agerberth, Birgitta; Gudmundsson, Gudmundur H. (2020): Host Directed Therapy Against Infection by Boosting Innate Immunity. In Front. Immunol. 11, p. 1209. DOI: 10.3389/fimmu.2020.01209.

Bessler, Wolfgang G.; Puce, Karola; vor dem Esche, Ulrich; Kirschning, Carsten; Huber, Maria (2009): Immunomodulating effects of OM-89, a bacterial extract from Escherichia coli, in murine and human leukocytes. In Arzneimittel-Forschung 59 (11), pp. 571–577. DOI: 10.1055/s-0031-1296446.

Blango, Matthew G.; Ott, Elizabeth M.; Erman, Andreja; Veranic, Peter; Mulvey, Matthew A. (2014): Forced resurgence and targeting of intracellular uropathogenic Escherichia coli reservoirs. In PloS one 9 (3), e93327. DOI: 10.1371/journal.pone.0093327.

Bongers, Suzanne; Hellebrekers, Pien; Leenen, Luke P. H.; Koenderman, Leo; Hietbrink, Falco (2019): Intracellular Penetration and Effects of Antibiotics on Staphylococcus aureus Inside Human Neutrophils: A Comprehensive Review. In Antibiotics (Basel, Switzerland) 8 (2). DOI: 10.3390/antibiotics8020054.

Canton, Tracy; Durand, Méline; Baulier, Edouard; Pasquali, Christian; Calin, Ruxandra; Ingersoll, Molly A.; Rousseau, Matthieu (2025): Oral OM-89 in combination with antibiotics prevents recurrent infection in a mouse model of urinary tract infection.

Carryn, Stéphane; Chanteux, Hugues; Seral, Cristina; Mingeot-Leclercq, Marie-Paule; van Bambeke, Françoise; Tulkens, Paul M. (2003): Intracellular pharmacodynamics of antibiotics. In Infectious disease clinics of North America 17 (3), pp. 615–634. DOI: 10.1016/S0891-5520(03)00066-7.

Chen, S. L.; Hung, C.-S.; Xu, J.; Reigstad, C. S.; Magrini, V.; Sabo, A. et al. (2006): Identification of genes subject to positive selection in uropathogenic strains of Escherichia coli: A comparative genomics approach. In Proceedings of the National Academy of Sciences 103 (15), pp. 5977–5982. DOI: 10.1073/pnas.0600938103.

Chifiriuc, Mariana Carmen; Holban, Alina Maria; Curutiu, Carmen; Ditu, Lia-Mara; Mihaescu, Grigore; Oprea, Alexandra Elena et al. (2016): Antibiotic Drug Delivery Systems for the Intracellular Targeting of Bacterial Pathogens. In Ali Demir Sezer (Ed.): Smart Drug Delivery System: InTech.

Cox, D.; Lee, D. J.; Dale, B. M.; Calafat, J.; Greenberg, S. (2000): A Rab11-containing rapidly recycling compartment in macrophages that promotes phagocytosis. In Proceedings of the National Academy of Sciences of the United States of America 97 (2), pp. 680–685. DOI: 10.1073/pnas.97.2.680.

Datsenko, K. A.; Wanner, B. L. (2000): One-step inactivation of chromosomal genes in Escherichia coli K-12 using PCR products. In Proceedings of the National Academy of Sciences 97 (12), pp. 6640–6645. DOI: 10.1073/pnas.120163297.

Dobin, Alexander; Davis, Carrie A.; Schlesinger, Felix; Drenkow, Jorg; Zaleski, Chris; Jha, Sonali et al. (2013): STAR: ultrafast universal RNA-seq aligner. In Bioinformatics (Oxford, England) 29 (1), pp. 15–21. DOI: 10.1093/bioinformatics/bts635.

Elsinghorst, E. A. (1994): Measurement of invasion by gentamicin resistance. In Methods in enzymology 236, pp. 405–420. DOI: 10.1016/0076-6879(94)36030-8.

Eshaghi, Majid; Mehershahi, Kurosh S.; Chen, Swaine L. (2016): Brighter Fluorescent Derivatives of UTI89 Utilizing a Monomeric vGFP. In Pathogens (Basel, Switzerland) 5 (1). DOI: 10.3390/pathogens5010003.

Eskelinen, Eeva-Liisa (2006): Roles of LAMP-1 and LAMP-2 in lysosome biogenesis and autophagy. In Molecular aspects of medicine 27 (5-6), pp. 495–502. DOI: 10.1016/j.mam.2006.08.005.

Eto, Danelle S.; Sundsbak, Jamie L.; Mulvey, Matthew A. (2006): Actin-gated intracellular growth and resurgence of uropathogenic Escherichia coli. In Cellular microbiology 8 (4), pp. 704–717. DOI: 10.1111/j.1462-5822.2006.00691.x.

Foxman, Betsy; Barlow, Robin; D'Arcy, Hannah; Gillespie, Brenda; Sobel, Jack D. (2000): Urinary Tract Infection. In Annals of Epidemiology 10 (8), pp. 509–515. DOI: 10.1016/s1047-2797(00)00072-7.

Frey, C.; Obolensky, W.; Wyss, H. (1986): Treatment of recurrent urinary tract infections: efficacy of an orally administered biological response modifier. In Urologia internationalis 41 (6), pp. 444–446. DOI: 10.1159/000281253.

Global burden of bacterial antimicrobial resistance 1990-2021: a systematic analysis with forecasts to 2050 (2024). In Lancet (London, England) 404 (10459), pp. 1199–1226.

Höger, P. H.; Seger, R. A.; Schaad, U. B.; Hitzig, W. H. (1985): Chronic granulomatous disease: uptake and intracellular activity of fosfomycin in granulocytes. In Pediatric research 19 (1), pp. 38–44. DOI: 10.1203/00006450-198501000-00011.

Huber, M.; Ayoub, M.; Pfannes, S. D.; Mittenbühler, K.; Weis, K.; Bessler, W. G.; Baier, W. (2000): Immunostimulatory activity of the bacterial extract OM-8. In European journal of medical research 5 (3), pp. 101–109.

Izumi, Tetsuro (2007): Physiological roles of Rab27 effectors in regulated exocytosis. In Endocrine journal 54 (5), pp. 649–657. DOI: 10.1507/endocrj.KR-78.

Jafari, Nazila V.; Rohn, Jennifer L. (2022): The urothelium: a multi-faceted barrier against a harsh environment. In Mucosal immunology 15 (6), pp. 1127–1142. DOI: 10.1038/s41385-022-00565-0.

Kadurugamuwa, J. L.; Beveridge, T. J. (1998): Delivery of the non-membrane-permeative antibiotic gentamicin into mammalian cells by using Shigella flexneri membrane vesicles. In Antimicrobial agents and chemotherapy 42 (6), pp. 1476–1483. DOI: 10.1128/AAC.42.6.1476.

Kamaruzzaman, Nor Fadhilah; Kendall, Sharon; Good, Liam (2017): Targeting the hard to reach: challenges and novel strategies in the treatment of intracellular bacterial infections. In British journal of pharmacology 174 (14), pp. 2225–2236. DOI: 10.1111/bph.13664.

Klein, Eric A.; Gitai, Zemer (2013): Draft Genome Sequence of Uropathogenic Escherichia coli Strain J96. In Genome announcements 1 (1). DOI: 10.1128/genomeA.00245-12.

Kolberg, Liis; Raudvere, Uku; Kuzmin, Ivan; Adler, Priit; Vilo, Jaak; Peterson, Hedi (2023): g:Profiler-interoperable web service for functional enrichment analysis and gene identifier mapping (2023 update). In Nucleic acids research 51 (W1), W207-W212. DOI: 10.1093/nar/gkad347.

Korotkevich, Gennady; Sukhov, Vladimir; Budin, Nikolay; Shpak, Boris; Artyomov, Maxim N.; Sergushichev, Alexey (2016): Fast gene set enrichment analysis.

Kumar, Anita V.; Mills, Joslyn; Lapierre, Louis R. (2022): Selective Autophagy Receptor p62/SQSTM1, a Pivotal Player in Stress and Aging. In Frontiers in cell and developmental biology 10, p. 793328. DOI: 10.3389/fcell.2022.793328.

Lambert, R. J.; Pearson, J. (2000): Susceptibility testing: accurate and reproducible minimum inhibitory concentration (MIC) and non-inhibitory concentration (NIC) values. In Journal of applied microbiology 88 (5), pp. 784–790. DOI: 10.1046/j.1365-2672.2000.01017.x.

Lewis, Adam J.; Richards, Amanda C.; Mulvey, Matthew A. (2016): Invasion of Host Cells and Tissues by Uropathogenic Bacteria. In Microbiology spectrum 4 (6). DOI: 10.1128/microbiolspec.uti-0026-2016.

Li, Hao; Rukina, Daria; David, Fabrice P. A.; Li, Terytty Yang; Oh, Chang-Myung; Gao, Arwen W. et al. (2019): Identifying gene function and module connections by the integration of multispecies expression compendia. In Genome research 29 (12), pp. 2034–2045. DOI: 10.1101/gr.251983.119.

Li, Xueping; Jiang, Lingyan; Zhang, Si; Zhou, Jiarui; Le Liu; Jin, Chen et al. (2024): Uropathogenic Escherichia coli Subverts Host Autophagic Defenses by Stalling Preautophagosomal Structures to Escape Lysosome Exocytosis. In The Journal of infectious diseases 230 (3), e548-e558. DOI: 10.1093/infdis/jiae063.

Mauthe, Mario; Orhon, Idil; Rocchi, Cecilia; Zhou, Xingdong; Luhr, Morten; Hijlkema, Kerst-Jan et al. (2018): Chloroquine inhibits autophagic flux by decreasing autophagosome-lysosome fusion. In Autophagy 14 (8), pp. 1435–1455. DOI: 10.1080/15548627.2018.1474314.

Mauvezin, Caroline; Neufeld, Thomas P. (2015): Bafilomycin A1 disrupts autophagic flux by inhibiting both V-ATPase-dependent acidification and Ca-P60A/SERCA-dependent autophagosome-lysosome fusion. In Autophagy 11 (8), pp. 1437–1438. DOI: 10.1080/15548627.2015.1066957.

Medina, Martha; Castillo-Pino, Edgardo (2019): An introduction to the epidemiology and burden of urinary tract infections. In Therapeutic advances in urology 11, 1756287219832172. DOI: 10.1177/1756287219832172.

Miao, Yuxuan; Bist, Pradeep; Wu, Jianxuan; Zhao, Qing; Li, Qi-Jing; Wan, Ying; Abraham, Soman N. (2017): Collaboration between Distinct Rab Small GTPase Trafficking Circuits Mediates Bacterial Clearance from the Bladder Epithelium. In Cell host & microbe 22 (3), 330-342.e4. DOI: 10.1016/j.chom.2017.08.002.

Miao, Yuxuan; Li, Guojie; Zhang, Xiaoli; Xu, Haoxing; Abraham, Soman N. (2015): A TRP Channel Senses Lysosome Neutralization by Pathogens to Trigger Their Expulsion. In Cell 161 (6), pp. 1306–1319. DOI: 10.1016/j.cell.2015.05.009.

Mobley, H. L.; Green, D. M.; Trifillis, A. L.; Johnson, D. E.; Chippendale, G. R.; Lockatell, C. V. et al. (1990): Pyelonephritogenic Escherichia coli and killing of cultured human renal proximal tubular epithelial cells: role of hemolysin in some strains. In Infection and immunity 58 (5), pp. 1281–1289. DOI: 10.1128/iai.58.5.1281-1289.1990.

Mulvey, M. A.; Schilling, J. D.; Hultgren, S. J. (2001): Establishment of a persistent Escherichia coli reservoir during the acute phase of a bladder infection. In Infection and immunity 69 (7), pp. 4572–4579. DOI: 10.1128/IAI.69.7.4572–4579.2001.

Murray, Christopher J. L.; Ikuta, Kevin Shunji; Sharara, Fablina; Swetschinski, Lucien; Robles Aguilar, Gisela; Gray, Authia et al. (2022): Global burden of bacterial antimicrobial resistance in 2019: a systematic analysis. In The Lancet 399 (10325), pp. 629–655. DOI: 10.1016/S0140-6736(21)02724-0.

Mysorekar, Indira U.; Hultgren, Scott J. (2006): Mechanisms of uropathogenic Escherichia coli persistence and eradication from the urinary tract. In Proceedings of the National Academy of Sciences of the United States of America 103 (38), pp. 14170–14175. DOI: 10.1073/pnas.0602136103.

Naskar, Manisha; Parekh, Viraj P.; Abraham, Mathew A.; Alibasic, Zehra; Kim, Min Jung; Suk, Gyeongseo et al. (2023): α-Hemolysin promotes uropathogenic E. coli persistence in bladder epithelial cells via abrogating bacteria-harboring lysosome acidification. In PLoS pathogens 19 (5), e1011388. DOI: 10.1371/journal.ppat.1011388.

Nisco, Nicole J. de; Neugent, Michael; Mull, Jason; Chen, Luming; Kuprasertkul, Amy; Souza Santos, Marcela de et al. (2019): Direct Detection of Tissue-Resident Bacteria and Chronic Inflammation in the Bladder Wall of Postmenopausal Women with Recurrent Urinary Tract Infection. In Journal of molecular biology 431 (21), pp. 4368–4379. DOI: 10.1016/j.jmb.2019.04.008.

Rosen, David A.; Hooton, Thomas M.; Stamm, Walter E.; Humphrey, Peter A.; Hultgren, Scott J. (2007): Detection of intracellular bacterial communities in human urinary tract infection. In PLoS medicine 4 (12), e329. DOI: 10.1371/journal.pmed.0040329.

Roth, Michael; Pasquali, Christian; Stolz, Daiana; Tamm, Michael (2017): Broncho Vaxom (OM-85) modulates rhinovirus docking proteins on human airway epithelial cells via Erk1/2 mitogen activated protein kinase and cAMP. In PloS one 12 (11), e0188010. DOI: 10.1371/journal.pone.0188010.

Sharma, Kunal; Thacker, Vivek V.; Dhar, Neeraj; Clapés Cabrer, Maria; Dubois, Anaëlle; Signorino-Gelo, François et al. (2021): Early invasion of the bladder wall by solitary bacteria protects UPEC from antibiotics and neutrophil swarms in an organoid model. In Cell reports 36 (3), p. 109351. DOI: 10.1016/j.celrep.2021.109351.

Simonet, Thomas; Rutschmann, Ophélie; Sharma, Kunal; Nass, Théo; Pavlou, Maria; Dubois, Anaëlle et al. (2022): High-content screening identifies a critical role for P pili in early adhesion of uropathogenic Escherichia coli to bladder cells.

Stracy, Mathew; Snitser, Olga; Yelin, Idan; Amer, Yara; Parizade, Miriam; Katz, Rachel et al. (2022): Minimizing treatment-induced emergence of antibiotic resistance in bacterial infections. In Science (New York, N.Y.) 375 (6583), pp. 889–894. DOI: 10.1126/science.abg9868.

Szulc-Dąbrowska, Lidia; Bossowska-Nowicka, Magdalena; Struzik, Justyna; Toka, Felix N. (2020): Cathepsins in Bacteria-Macrophage Interaction: Defenders or Victims of Circumstance? In Frontiers in cellular and infection microbiology 10, p. 601072. DOI: 10.3389/fcimb.2020.601072.

Tanida, Isei; Ueno, Takashi; Kominami, Eiki (2008): LC3 and Autophagy. In Methods in molecular biology (Clifton, N.J.) 445, pp. 77–88. DOI: 10.1007/978-1-59745-157-4_4.

Tulkens, P.; Trouet, A. (1978): The uptake and intracellular accumulation of aminoglycoside antibiotics in lysosomes of cultured rat fibroblasts. In Biochemical pharmacology 27 (4), pp. 415–424. DOI: 10.1016/0006-2952(78)90370-2.

Underwood, Rachel; Wang, Bing; Carico, Christine; Whitaker, Robert H.; Placzek, William J.; Yacoubian, Talene A. (2020): The GTPase Rab27b regulates the release, autophagic clearance, and toxicity of α-synuclein. In The Journal of biological chemistry 295 (23), pp. 8005–8016. DOI: 10.1074/jbc.RA120.013337.

van Dijk, A. (1982): 14C-OM 89: Absorption, distribution, elimination and excertion after single oral administration to the rat.

Vanlandingham, Phillip A.; Ceresa, Brian P. (2009): Rab7 regulates late endocytic trafficking downstream of multivesicular body biogenesis and cargo sequestration. In The Journal of biological chemistry 284 (18), pp. 12110–12124. DOI: 10.1074/jbc.M809277200.

Wright, Kelly J.; Seed, Patrick C.; Hultgren, Scott J. (2007): Development of intracellular bacterial communities of uropathogenic Escherichia coli depends on type 1 pili. In Cellular microbiology 9 (9), pp. 2230–2241. DOI: 10.1111/j.1462-5822.2007.00952.x.

Zulk, Jacob J.; Robertson, Clare M.; Ottinger, Samantha; Kambal, Amal; Tostado, Alejandra Rivera; Fleck, Rachel C. et al. (2025): Human bladder organoids model urinary tract infection and bacteriophage therapy. In bioRxiv: the preprint server for biology. DOI: 10.1101/2025.07.30.667685.

Figure 1

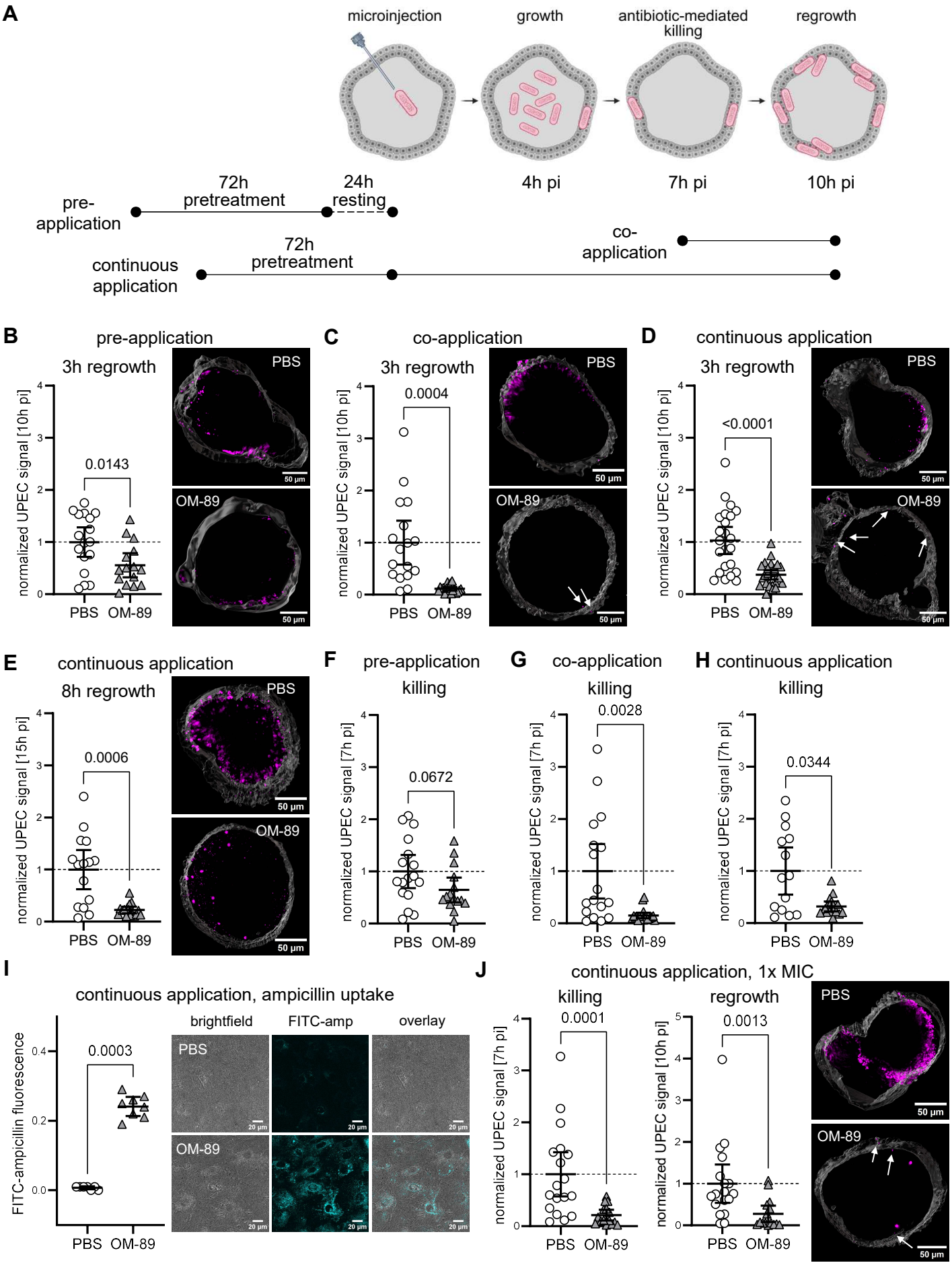
A
microinjection
growth
antibiotic-mediated killing
regrowth
4h pi
7h pi
10h pi
pre-application
72h pretreatment
24h resting
continuous application
72h pretreatment
co-application
B
pre-application
3h regrowth
normalized UPEC signal [10h pi]
0.0143
PBS
OM-89
C
co-application
3h regrowth
0.0004
D
continuous application
3h regrowth
<0.0001
E
continuous application
8h regrowth
normalized UPEC signal [15h pi]
0.0006
F
pre-application
killing
normalized UPEC signal [7h pi]
0.0672
G
co-application
killing
0.0028
H
continuous application
killing
0.0344
I
continuous application, ampicillin uptake
FITC-ampicillin fluorescence
0.0003
brightfield
FITC-amp
overlay
J
continuous application, 1x MIC
killing
0.0001
regrowth
0.0013
50 µm
20 µm

Figure 1. OM-89 reduces regrowth of CFT073 in mouse bladder organoids due to enhanced antibiotic-mediated killing.

(A) Mouse bladder organoids treated with OM-89 under different regimes (pre-application: OM-89 exposure for 72h and 24h rest period; co-application: OM-89 exposure together with antibiotic treatment; continuous application: OM-89 exposure both 72h before microinjection and throughout the entire experiment). After microinjection of fluorescently labelled UPEC (0h post-infection, pi), bacterial growth (4h pi), antibiotic-mediated killing (7h pi), and regrowth 3 hours after antibiotic withdrawal (10h pi) were monitored.
(B)-(D) CFT073 signal 10h pi (3h regrowth) at 10x MIC in (B) pre-application, (C) co-application, and (D) continuous application regimes in mouse bladder organoids. Each dot represents one organoid. Values normalized to PBS control (dashed line). Mean ± 95% CI. Welch's t test. N ≥ 15 per condition for (B), n ≥ 17 per condition for (C) and n ≥ 23 per condition for (D). Images show representative organoids (grey, surface reconstruction) and UPEC (magenta, some marked with arrows).
(E) CFT073 signal 15h pi (8h regrowth) at 10x MIC in the continuous application regime in mouse bladder organoids. Values normalized to PBS control (dashed line). Mean ± 95% CI. Mann-Whitney test. N ≥ 15 per condition. Images show representative organoids (grey, surface reconstruction) and UPEC (magenta, some marked with arrows).
(F)-(H) CFT073 signal 7h pi (killing) at 10x MIC in (F) pre-application, (G) co-application, and (H) continuous application regimes in mouse bladder organoids. Values normalized to PBS control (dashed line). Mean ± 95% CI. Welch's t test for (F), Mann-Whitney test for (G), (H). N ≥ 15 per condition for (F), n ≥ 17 per condition for (G) and n ≥ 14 per condition for (H).
(I) FITC-labelled ampicillin uptake into monolayers of mouse bladder epithelial cells during the continuous application regime. Quantification of fluorescence after background subtraction of PBS- or OM-89-treated cells without labelled antibiotic. Each dot represents one field of view. Mean ± 95% CI. Mann-Whitney test. N ≥ 7 per condition. Z-projection (maximum intensity) of representative images. FITC-ampicillin shown in cyan.
(J) CFT073 signal 7h pi (1x MIC; killing and 10h pi (regrowth) in mouse bladder organoids during the continuous application regime. Each dot represents one organoid. Values normalized to PBS control (dashed line). Mean ± 95% CI. Mann-Whitney test. N ≥ 15 per condition. Images show representative organoids (grey, surface reconstruction) and UPEC (magenta, some marked with arrows).

Figure 2

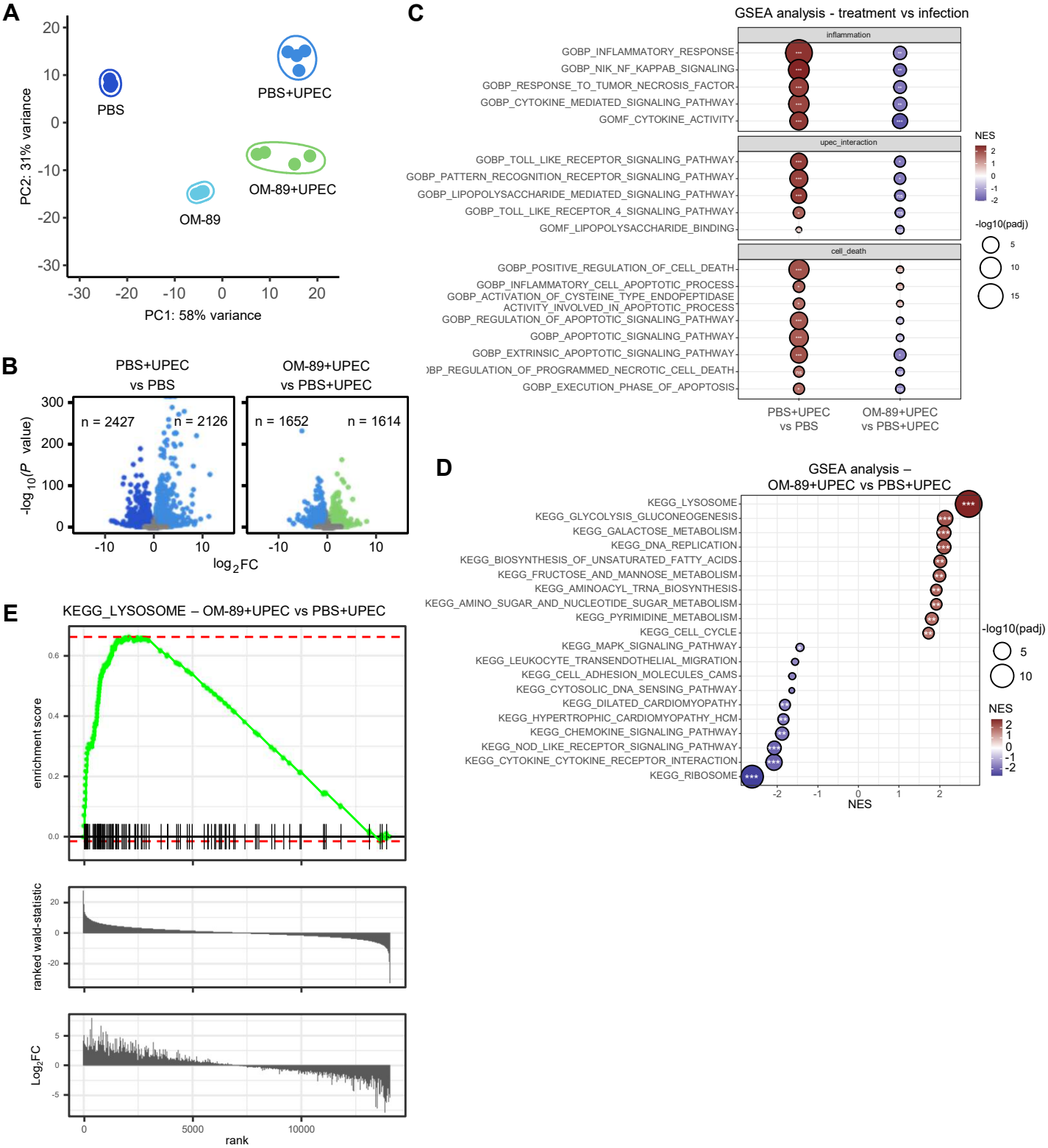
A
PBS
PBS+UPEC
OM-89
OM-89+UPEC
PC2: 31% variance
PC1: 58% variance
B
PBS+UPEC vs PBS
OM-89+UPEC vs PBS+UPEC
n = 2427
n = 2126
n = 1652
n = 1614
-log10(P value)
log2FC
C
GSEA analysis - treatment vs infection
inflammation
GOBP_INFLAMMATORY_RESPONSE
GOBP_NIK_NF_KAPPAB_SIGNALING
GOBP_RESPONSE_TO_TUMOR_NECROSIS_FACTOR
GOBP_CYTOKINE_MEDIATED_SIGNALING_PATHWAY
GOMF_CYTOKINE_ACTIVITY
upec_interaction
GOBP_TOLL_LIKE_RECEPTOR_SIGNALING_PATHWAY
GOBP_PATTERN_RECOGNITION_RECEPTOR_SIGNALING_PATHWAY
GOBP_LIPOPOLYSACCHARIDE_MEDIATED_SIGNALING_PATHWAY
GOBP_TOLL_LIKE_RECEPTOR_4_SIGNALING_PATHWAY
GOMF_LIPOPOLYSACCHARIDE_BINDING
cell_death
GOBP_POSITIVE_REGULATION_OF_CELL_DEATH
GOBP_INFLAMMATORY_CELL_APOPTOTIC_PROCESS
GOBP_ACTIVATION_OF_CYSTEINE_TYPE_ENDOPEPTIDASE ACTIVITY_INVOLVED_IN_APOPTOTIC_PROCESS
GOBP_REGULATION_OF_APOPTOTIC_SIGNALING_PATHWAY
GOBP_APOPTOTIC_SIGNALING_PATHWAY
GOBP_EXTRINSIC_APOPTOTIC_SIGNALING_PATHWAY
GOBP_REGULATION_OF_PROGRAMMED_NECROTIC_CELL_DEATH
GOBP_EXECUTION_PHASE_OF_APOPTOSIS
PBS+UPEC vs PBS
OM-89+UPEC vs PBS+UPEC
NES
-log10(padj)
D
GSEA analysis – OM-89+UPEC vs PBS+UPEC
KEGG_LYSOSOME
KEGG_GLYCOLYSIS_GLUCONEOGENESIS
KEGG_GALACTOSE_METABOLISM
KEGG_DNA_REPLICATION
KEGG_BIOSYNTHESIS_OF_UNSATURATED_FATTY_ACIDS
KEGG_FRUCTOSE_AND_MANNOSE_METABOLISM
KEGG_AMINOACYL_TRNA_BIOSYNTHESIS
KEGG_AMINO_SUGAR_AND_NUCLEOTIDE_SUGAR_METABOLISM
KEGG_PYRIMIDINE_METABOLISM
KEGG_CELL_CYCLE
KEGG_MAPK_SIGNALING_PATHWAY
KEGG_LEUKOCYTE_TRANSENDOTHELIAL_MIGRATION
KEGG_CELL_ADHESION_MOLECULES_CAMS
KEGG_CYTOSOLIC_DNA_SENSING_PATHWAY
KEGG_DILATED_CARDIOMYOPATHY
KEGG_HYPERTROPHIC_CARDIOMYOPATHY_HCM
KEGG_CHEMOKINE_SIGNALING_PATHWAY
KEGG_NOD_LIKE_RECEPTOR_SIGNALING_PATHWAY
KEGG_CYTOKINE_CYTOKINE_RECEPTOR_INTERACTION
KEGG_RIBOSOME
NES
-log10(padj)
E
KEGG_LYSOSOME – OM-89+UPEC vs PBS+UPEC
enrichment score
ranked wald-statistic
Log2FC
rank

Figure 2. OM-89 modulates inflammatory signaling and promotes lysosomal pathways in bladder epithelial cells.

(A) Principal component analysis (PCA) of mouse bladder organoids treated with OM-89 or PBS, with and without CFT073 infection (PBS – dark blue, OM-89 – cyan, PBS+UPEC – light blue, OM-89+UPEC – green).
(B) Volcano plots of differentially expressed genes ($\log_2 FC \geq 1$; adjusted $p \leq 0.05$) comparing PBS-treated organoids with (light blue) and without infection (dark blue), and OM-89- (green) versus PBS-treated organoids during infection (light blue).
(C) Gene set enrichment analysis (GSEA) of treatment and infection groups. GO-BP terms were clustered into infection-relevant pathways. NES, normalized enrichment score. Non-significant changes not highlighted.
(D) GSEA of the top 10 Kyoto Encyclopedia of Genes and Genomes (KEGG) terms comparing OM-89- and PBS-treated organoids during infection. Ns changes not highlighted
(E) Enrichment plot of lysosomal pathway genes (KEGG term) in OM-89- versus PBS-treated organoids during infection (FDR corrected p-value = 1.88e-14 and uncorrected p-value = 1.21e-16).
(A)-(E) Data from four independent wells with $n \geq 50$ organoids each.

Figure 3

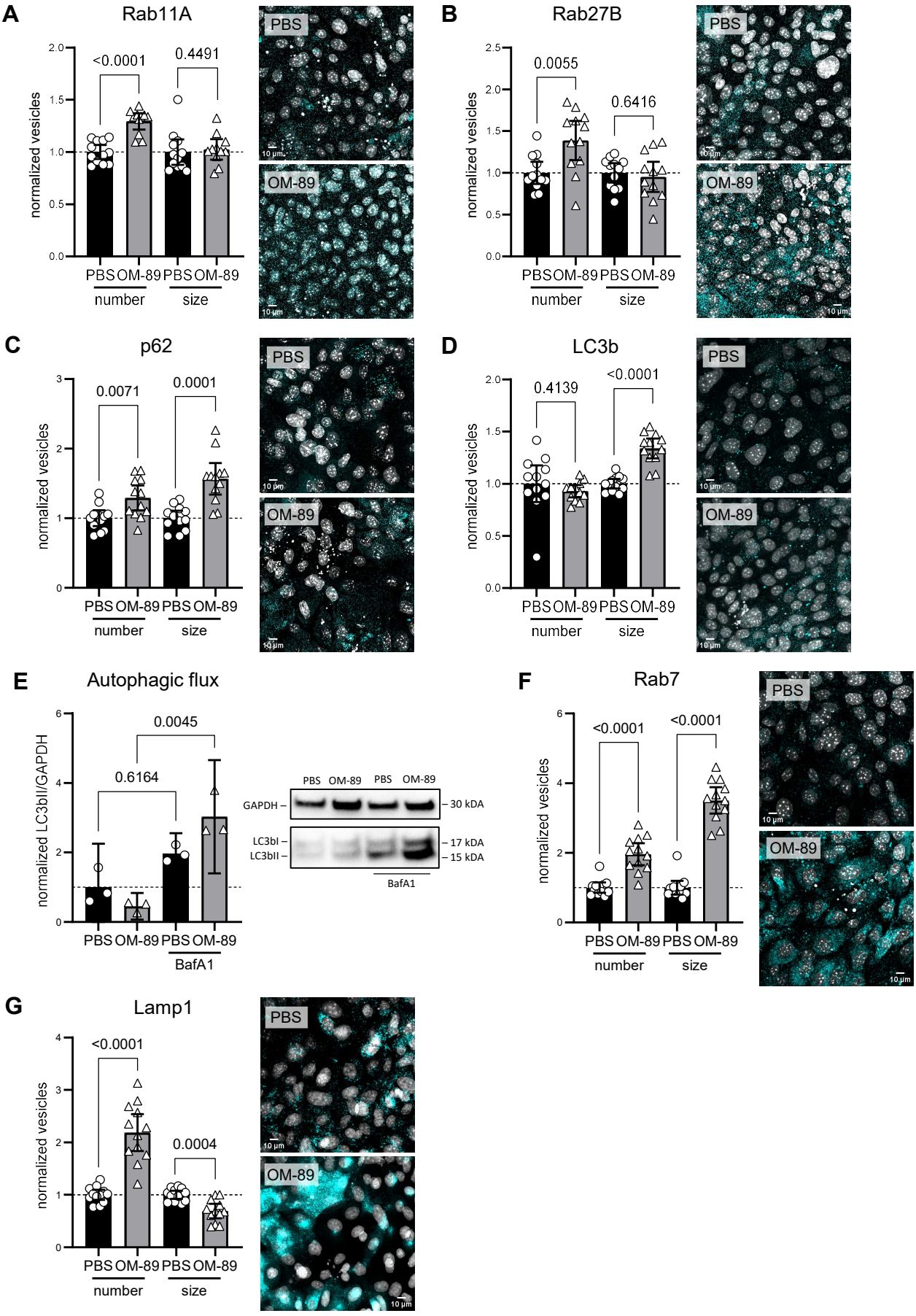
A
Rab11A
normalized vesicles
<0.0001
0.4491
PBS OM-89 PBS OM-89
number
size
PBS
OM-89
B
Rab27B
0.0055
0.6416
C
p62
0.0071
0.0001
D
LC3b
0.4139
<0.0001
E
Autophagic flux
normalized LC3bII/GAPDH
0.0045
0.6164
BafA1
GAPDH
LC3bI
LC3bII
30 kDA
17 kDA
15 kDA
F
Rab7
G
Lamp1
0.0004
10 µm

Figure 3. OM-89 remodels vesicle organization and turnover in bladder epithelial cells during UPEC infection.

(A)-(D), (F), (G) Quantification of vesicle numbers and size for (A) Rab11A, (B) Rab27B, (C) p62, (D) LC3b, (F) Rab7, and (G) Lamp1 in infected monolayers of mouse bladder epithelial cells with and without OM-89 treatment. Values normalized to PBS control (dashed line). Mean ± 95% CI. Mann-Whitney test for Rab11A and Rab7 (A), (F); Welch's t test for Rab27B, p62, LC3b and Lamp1 (B)-(D), (G). N = 12 per condition. Z-projection (maximum intensity) of representative images. Foci, cyan; DAPI, grey.
(E) Western blot analysis of LC3b during infection of monolayers. LC3b-II/Gapdh ratio normalized to PBS control (dashed line). Mean ± 95% CI. Kruskal-Wallis test with Dunn's correction. Autophagic flux (BafA1-blocked minus unblocked LC3b-II/Gapdh): PBS = 24.75 ± 10.68; OM-89 = 65.87 ± 9.11. N = 3 per condition.

Figure 4

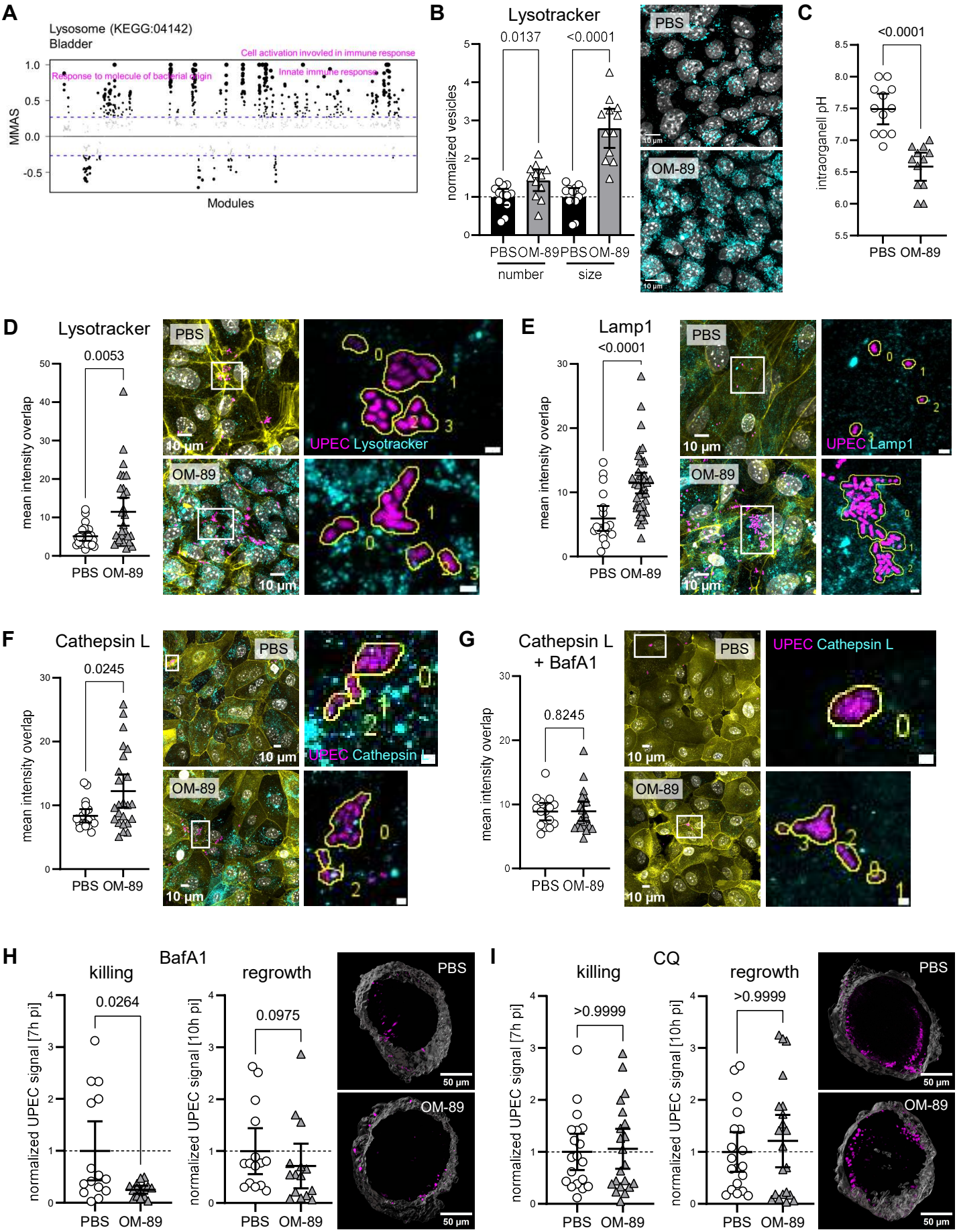
A
Lysosome (KEGG:04142)
Bladder
Cell activation involved in immune response
Response to molecule of bacterial origin
Innate immune response
MMAS
Modules
B
Lysotracker
0.0137
<0.0001
normalized vesicles
PBS OM-89 PBS OM-89
number
size
PBS
OM-89
C
<0.0001
intraorganell pH
PBS OM-89
D
Lysotracker
0.0053
mean intensity overlap
PBS OM-89
PBS
OM-89
10 µm
UPEC Lysotracker
E
Lamp1
<0.0001
mean intensity overlap
PBS OM-89
PBS
OM-89
10 µm
UPEC Lamp1
F
Cathepsin L
0.0245
mean intensity overlap
PBS OM-89
PBS
OM-89
10 µm
UPEC Cathepsin L
G
Cathepsin L
+ BafA1
0.8245
mean intensity overlap
PBS OM-89
PBS
OM-89
10 µm
UPEC Cathepsin L
H
BafA1
killing
0.0264
normalized UPEC signal [7h pi]
PBS OM-89
regrowth
0.0975
normalized UPEC signal [10h pi]
PBS OM-89
PBS
OM-89
50 µm
I
CQ
killing
>0.9999
normalized UPEC signal [7h pi]
PBS OM-89
regrowth
>0.9999
normalized UPEC signal [10h pi]
PBS OM-89
PBS
OM-89
50 µm

Figure 4. OM-89 enhances lysosomal activity and acidification, and disruption of acidification alters UPEC clearance.

(A) GeneBridge MMAS (Module-Module Association Score) analysis of KEGG lysosomal terms in human bladder datasets. Positively correlated modules linked to immune responses and bacterial defense are highlighted.
(B) Quantification of vesicle numbers and size of LysoTracker DND-99 in infected monolayers of mouse bladder epithelial cells with and without OM-89 treatment. Values normalized to PBS controls (dashed line). Mean ± 95% CI. Vesicle numbers analyzed with Welch's t test; vesicle size with Mann-Whitney test. N = 12 per condition.
(C) Intraorganelle pH in infected monolayers with and without OM-89 treatment. Mean ± 95% CI. Welch's t test. N = 12 per condition.
(D)-(G) Co-localization of intracellular UPEC with (D) LysoTracker, (E) Lamp1, (F) Cathepsin L and (G) Cathepsin L with bafilomycin A1 (BafA1) blocking in monolayers of mouse bladder epithelial cells. Intensities normalized to ROI area. Mann-Whitney test. N ≥ 24 per condition for LysoTracker, n ≥ 18 per condition for Lamp1, n ≥ 19 per condition for Cathepsin L, n ≥ 15 per condition for Cathepsin L + BafA1 blocking. Enrichment score (= observed overlap/random overlap) between OM-89 vs PBS for (D) 0.68 vs 0.71, (E) 0.94 vs 0.89, (F) 1.25 vs 0.91 and (G) 1.06 vs 1.17. Random overlap from SI Figure 4B-D, F. Z-projection (maximum intensity) of representative images. (D), (E) Phalloidin, yellow; (F), (G) CellMask, yellow; (D), (E) DAPI, grey; (F), (G) Hoechst, grey; (D)-(G) UPEC, magenta; LysoTracker/Lamp1/Cathepsin L, cyan. Insets: intracellular UPEC (highlighted squares) with ROIs used for intensity quantification (scale bar of inserts, 2 µm).
(H), (I) CFT073 signal 7h pi (killing) and 10 h pi (regrowth) in mouse bladder organoids after blocking with (H) BafA1 or (I) CQ. Each dot represents one organoid. Values normalized to PBS control (dashed line). Mean ± 95% CI. Mann-Whitney test. N = 15 per condition. Images show representative organoids (grey, surface reconstruction) and UPEC (magenta, some marked with arrows).

Figure 5

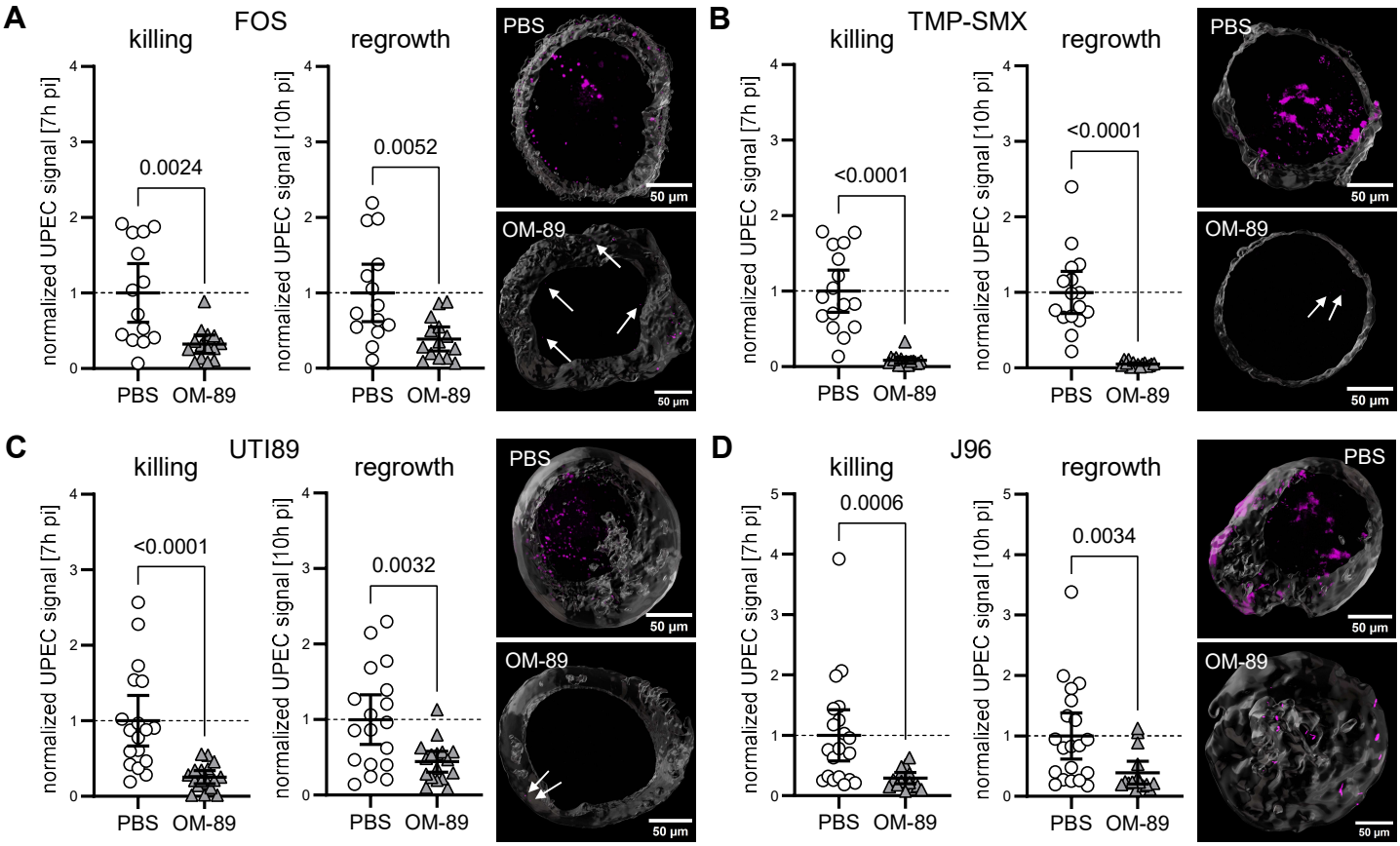
A
FOS
killing
regrowth
normalized UPEC signal [7h pi]
normalized UPEC signal [10h pi]
0.0024
0.0052
PBS
OM-89
PBS
OM-89
50 µm
B
TMP-SMX
killing
regrowth
<0.0001
<0.0001
C
UTI89
<0.0001
0.0032
D
J96
0.0006
0.0034

Figure 5. OM-89 reduces UPEC recurrence in bladder organoids across antibiotics and strains.

(A), (B) CFT073 signal during treatment with (A) Fosfomycin (FOS) or (B) trimethoprim-sulfamethoxazole (TMP-SMX). Quantification of bacterial fluorescence area in mouse bladder organoids 7h pi (killing) and 10h pi (regrowth). Each dot represents one organoid. Values normalized to PBS control (dashed line). Mean ± 95% CI. Mann-Whitney test for killing in (B); Welch's t test for (A) and regrowth in (B). N ≥ 14 per condition for (A) and n ≥ 15 per condition for (B). Representative organoids shown (grey, surface reconstruction) with UPEC (magenta, some marked with arrows).
(C)-(D) Regrowth of (C) UTI89 and (D) J96 after ampicillin treatment (10x strain-specific MIC). Quantification of bacterial fluorescence area 7h pi (killing) and 10h pi (regrowth). Each dot represents one organoid. Values normalized to PBS control (dashed line). Mean ± 95% CI. Mann-Whitney test for killing in (C), (D) and regrowth in (D); Welch's t test for regrowth in (C). N ≥ 17 per condition for (C) and n ≥ 15 per condition for (D). Representative organoids shown (grey, surface reconstruction) with UPEC (magenta, some marked with arrows).

Supplementary Figure 1

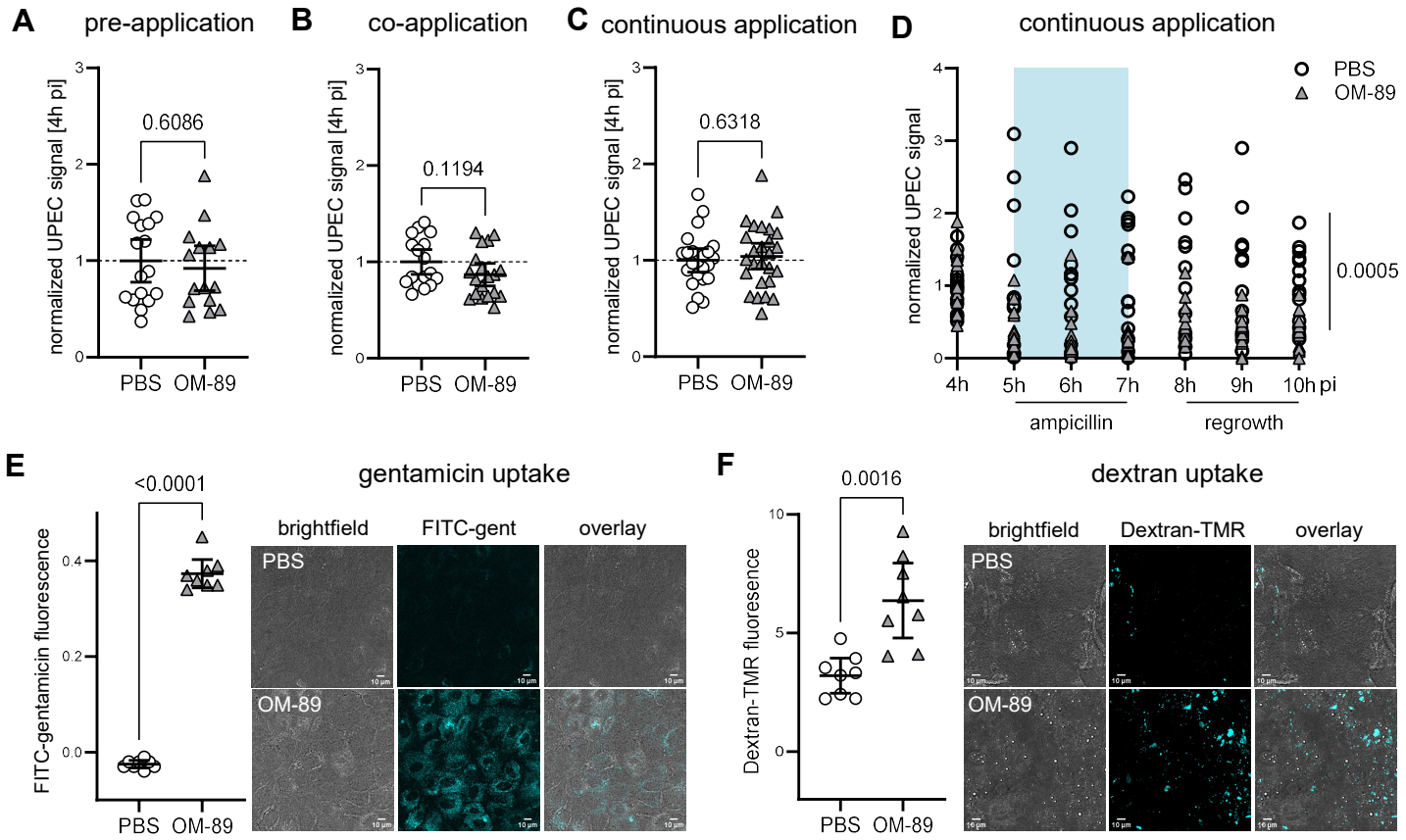

SI Figure 1. OM-89 enhances antibiotic uptake in bladder epithelial cells.

(A-C) Mouse bladder organoids treated with OM-89 under (A) pre-application, (B) co-application, or (C) continuous application regimes. Quantification of CFT073 fluorescence area at 4h post-infection (pi). Each dot represents one organoid. Values normalized to PBS control (dashed line). Mean ± 95% CI. Welch's t test. N ≥ 15 per condition for (A), n ≥ 17 per condition for (B) and n ≥ 23 per condition for (C).
(D) CFT073 signal over time in the continuous application regime. Quantification of bacterial fluorescence area normalized to PBS-treated organoids at the same timepoint. Each dot represents one organoid, lines connect matched organoids. RM two-way ANOVA with Šídák's correction; p-value shown for treatment effect. N ≥ 14 per condition.
(E), (F) Uptake of (E) FITC-labeled gentamicin and (F) Dextran-TMR in mouse bladder epithelial cell monolayers. Quantification of fluorescence after background subtraction of PBS- or OM-89-treated cells without labeled antibiotic. Mean ± 95% CI. Welch's test. N = 8 per condition. Z-projection (maximum intensity) of representative images. FITC-gentamicin and Dextran-TMR shown in cyan

Supplementary Figure 2

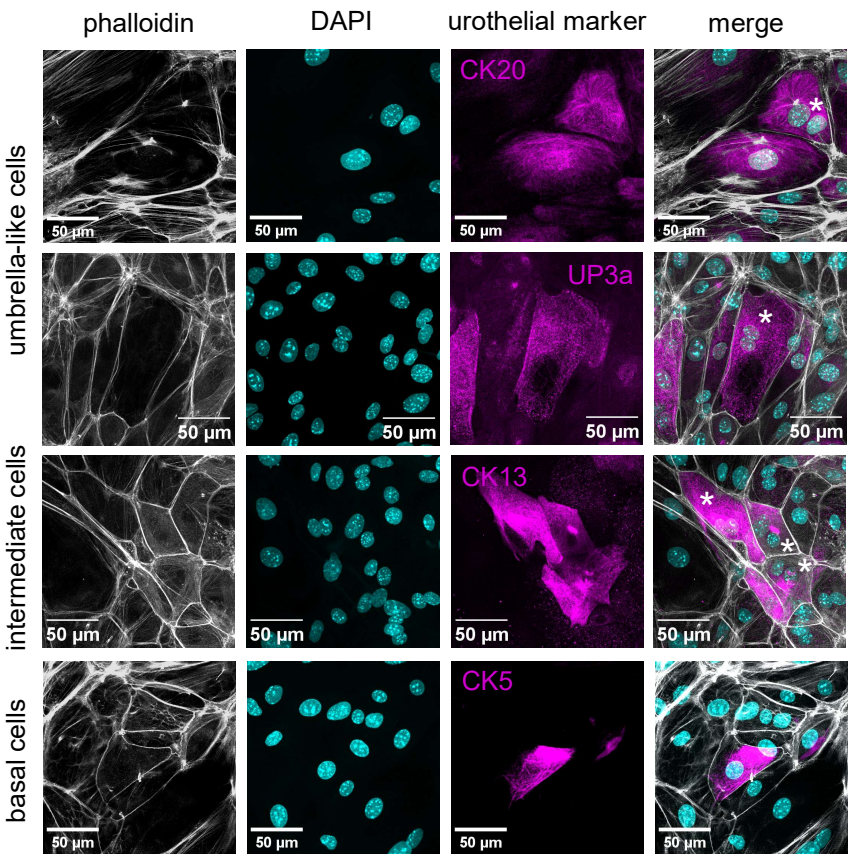

SI Figure 2. Establishment of differentiated mouse bladder epithelial cell monolayer.

Staining of differentiated mouse monolayer for bladder epithelial cell markers: Cytokeratin (CK) 20 – umbrella-like cells. Uroplakin (UP) 3a – umbrella-like cells. CK13 – intermediate cells. CK13-positive, binucleated cells indicate late intermediate cells. CK5 – basal cells. Binucleated cells indicated with asterisk.

Supplementary Figure 3

A

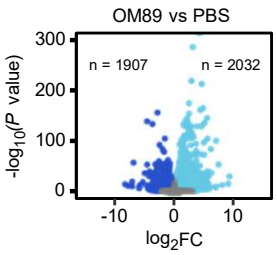

B

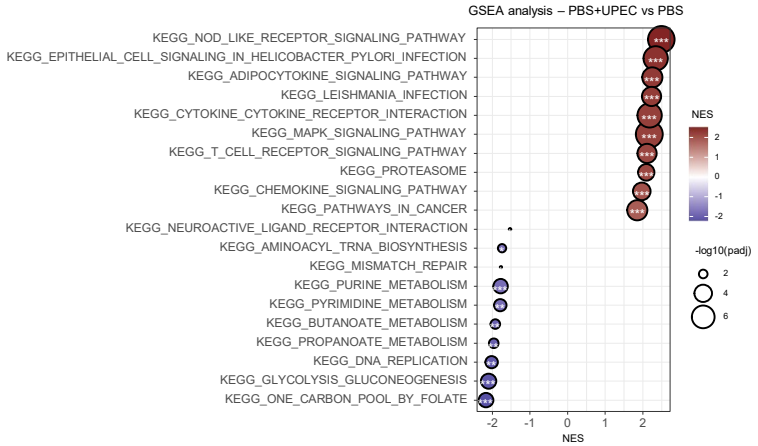

C

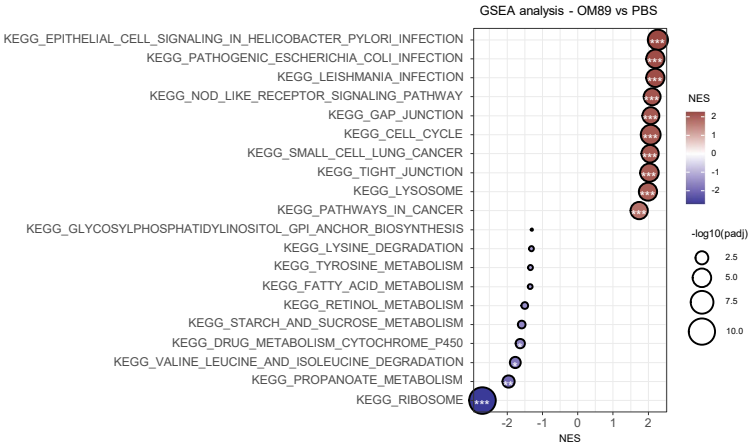

SI Figure 3. Transcriptomic analysis of OM-89-treated bladder organoids.

(A) Volcano plots of differentially expressed genes ($log_2FC \geq 1$; adjusted $p \leq 0.05$) comparing OM-89- (cyan) and PBS-treated organoids without infection (dark blue).
(B) Gene set enrichment analysis (GSEA) of the top 10 Kyoto Encyclopedia of Genes and Genomes (KEGG) terms comparing infection vs no infection in PBS control organoids. NES, normalized enrichment score. Ns changes not highlighted.
(C) GSEA of the top 10 KEGG terms comparing OM-89- and PBS-treated organoids without infection. Ns changes not highlighted
(A-C) Data from four independent wells with $n \geq 50$ organoids each.

Supplementary Figure 4

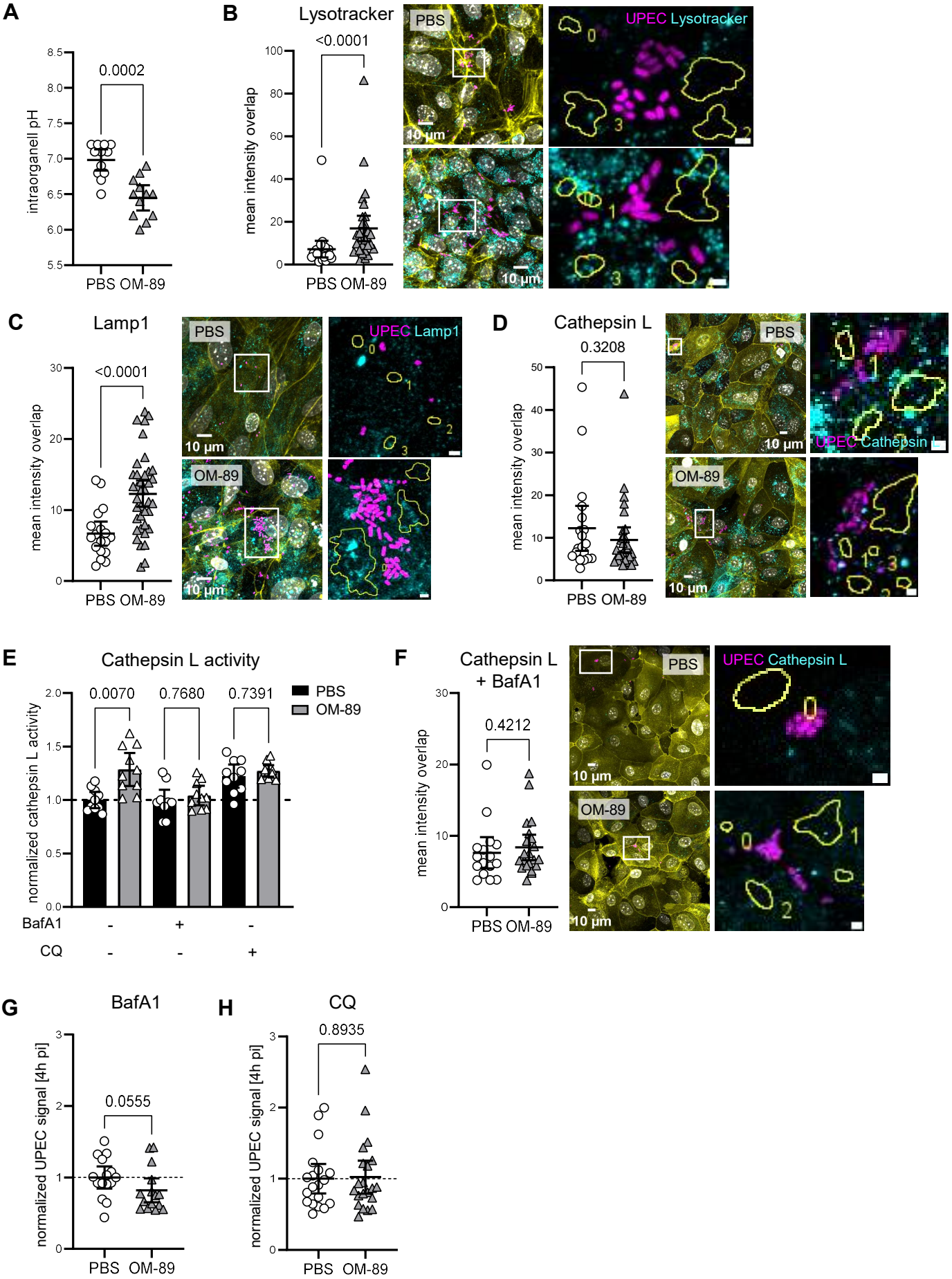

SI Figure 4. Controls and complementary analyses for lysosomal activity and blocking experiments.

(A) Intraorganelle pH in uninfected monolayers with and without OM-89 treatment. Mean ± 95% CI. Mann-Whitney test. N = 12 per condition.
(B)-(D), (F) Co-localization of random regions of interest (ROIs) with (B) LysoTracker, (C) Lamp1, (D) Cathepsin L and (F) Cathepsin L with bafilomycin A1 (BafA1) in monolayers of mouse bladder epithelial cells. Intensities normalized to ROI area. (B), (D), (F) Mann-Whitney test. (C) Welch's test. N ≥ 24 per condition for (B), n ≥ 18 per condition for (C), n ≥ 19 per condition for (D) and n ≥ 16 per condition for (F). Z-projection (maximum intensity) of representative images. (B), (C) Phalloidin, yellow; (D), (F) CellMask, yellow; (B), (C) DAPI, grey; (D), (F) Hoechst, grey; (B)-(D), (F) UPEC, magenta; LysoTracker/Lamp1/Cathepsin L, cyan. Insets: random ROIs used for intensity quantification (scale bar of inserts, 2 µm). Data correspond to Figure 4D-G.
(E) Cathepsin L activity during infection with or without OM-89, and with BafA1 or chloroquine (CQ) blocking. Values normalized to unblocked PBS controls (dashed line). Mean ± 95% CI. Brown-Forsythe ANOVA with Welch's correction. N = 10 per condition.
(G), (H) CFT073 growth after (G) BafA1 and (H) CQ blocking. Quantification of bacterial fluorescence area inside organoids 4h pi. Each dot represents one organoid. Values normalized to PBS control (dashed line). Mean ± 95% CI. Mann-Whitney test. N ≥ 15 per condition for (G) and n ≥ 19 per condition for (H).

Supplementary Figure 5

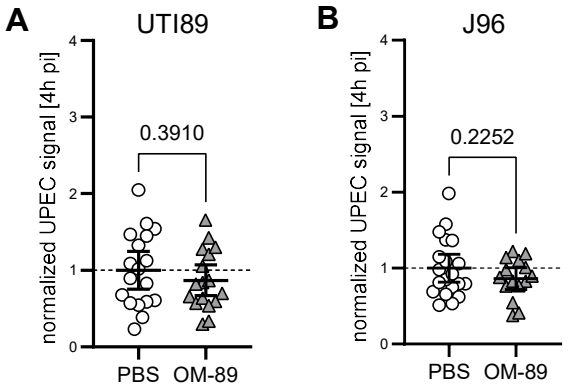

SI Figure 5. Growth of different laboratory UPEC strains in mouse bladder organoids.

(A), (B) Growth of lab UPEC strain (A) UTI89 and (B) J96. Quantification of bacterial fluorescence area inside organoids at 4h pi. Each dot represents one organoid. Values normalized to PBS control (dashed line). Mean ± 95% CI. Welch's test. N ≥ 17 per condition for (A) and n ≥ 15 per condition for (B).